Differentiation of cortical brain organoids and optic nerve-like structures from retinal confluent cultures of pluripotent stem cells.

1   Milan Fernando[1,#], Scott Lee[1,#], Jesse R. Wark[1,2], Di Xiao[3,4,5], Hani J. Kim[3,4,5], Grady C. Smith[1], Ted
2   Wong[6], Erdahl T. Teber[5,6], Robin R. Ali[7,8], Pengyi Yang[3,4,5], Mark E. Graham[2,5], Anai Gonzalez-
3   Cordero[1,5,*].
4
5   [1]Stem Cell Medicine Group, [2]Synapse Proteomics, [3]Computational Systems Biology Group,
6   [6]Bioinformatics; Children's Medical Research Institute, University of Sydney, Westmead, 2145, NSW,
7   Australia; [4]Charles Perkins Centre, School of Mathematics and Statistics, University of Sydney, Sydney,
8   NSW 2006, Australia; [5]School of Medical Sciences, Faculty of Medicine and Health, University of
9   Sydney, NSW 2006; [7]Gene and Cell Therapy Group, UCL Institute of Ophthalmology, London EC1V
10 9EL, UK. [8]Current address: Centre for Cell and Gene Therapy, King's College London, 8th Floor Tower
11 Wing, Guy's Hospital, London SE1 9RT, UK.
12
13 #these two authors contributed equally to the work
14
15 **Corresponding author:** Dr Anai Gonzalez Cordero
16 agonzalez-cordero@cmri.org.au
17 Stem Cell Medicine Group, Children's Medical Research Institute and University of Sydney
18 214 Hawkesbury Road, Westmead, 2145, NSW, Australia
19 Tel: +61 (2) 8865 2980

20
21 **Running title:** Cortical brain organoids from confluent iPS cell cultures
22
23 **Key worlds:** brain organoids, retinal organoids, pluripotent stem cells, omics, multi electrode array,
24 optic nerve

25

26

27

28

29

Abstract

Advances in the study of neurological conditions have been possible due to induced pluripotent stem cell technologies and the generation of neural cell types and organoids. Numerous studies have described the generation of neural ectoderm-derived retinal and brain structures from pluripotent stem cells. However, the field is still troubled by technical challenges, including high culture costs and organoid-to-organoid variability. Here, we describe a simple and economical protocol that reproducibly gives rise to the neural retina and cortical brain regions from confluent cultures of stem cells. The spontaneously generated cortical organoids were isolated and cultured in suspension conditions for maturation and are transcriptionally comparable to organoids generated by other methods and to human foetal cortex. Furthermore, these organoids show spontaneous functional network activity with proteomic analysis and electron microscopy demonstrating the presence of synaptic components and maturity. The generation of retinal and brain organoids in close proximity also enabled their mutual isolation. Further culture of this complex organoid system demonstrated the formation of optic nerve-like structures connecting retinal and brain organoids, which might facilitate the investigation of the mechanisms of neurological diseases of the eye and brain.

Introduction

The rapidly progressing field of human pluripotent stem cells (hPSCs), including embryonic (ES) and induced pluripotent stem (iPS) cells, and their derivative organoids continue to provide new insights into basic biology, human development, modelling of human diseases and discovery of innovative treatments. Neural differentiation, in particular, has been extensively studied, improving our understanding of the mechanism of neurodevelopmental conditions[1,2,3]. Large numbers of neurons and astrocytes are able to be generated using two-dimensional (2D) cultures derived from hPSCs[4,5] and these classical differentiation cultures were later optimised to three-dimensional (3D) suspension methods that better recapitulate the physiological niche and environment of the developing human brain[6].

In the developing central nervous system (CNS), the eye and the brain form as an extension of the forebrain diencephalic and telencephalic region, respectively[7]. Developmental biology studies have helped infer the molecular basis of this patterning process and facilitated the establishment of numerous differentiation protocols, which generate miniaturised versions of 3D organoids from PSCs. Brain organoids replicate specific brain regions or whole cerebral areas, with both occasionally developing eye regions[8] [9,10].

2

64 Differentiation protocols are usually classified as either guided/direct or non-guided/undirected cultures,
65 based on the necessity for guided differentiation using growth factors or their absence in non-guided
66 spontaneous differentiation, which relies on endogenous self-forming ability of the cells[11]. Brain
67 organoids generated using these varied methodologies have been comprehensively characterised
68 using transcriptome analysis by RNA sequencing. Single cell RNA sequencing (scRNA-seq) has
69 elucidated the cellular composition of organoids and reproducibility of organoid protocols[12,13,1,10,14-16].
70 However, the differentiation of PSC-derived brain organoids presents challenges, such as variability
71 within and between organoid batches and high culture costs. This lack of reproducibility demonstrates
72 the necessity of novel differentiation approaches. Furthermore, unbiased omics, including proteome
73 studies, together with robust measurements of neuronal activity, are critical to establish organoid
74 variability, maturation and functionality.

75

76 Diseases of the eye and the brain are now understood to be more intertwined than previously thought.
77 Studies of common conditions, such as Alzheimer's disease and glaucoma have demonstrated
78 neurodegenerative changes and disease traits in both brain and eye regions[17,18]. Complex organoids
79 have the potential to provide useful models of these human disease *in vitro* with the proviso that they
80 faithfully recapitulate retinal development, morphology and maturation. Therefore, improved formation
81 of hPSC-derived retinal-brain connection through an optic nerve is essential for effective degenerative
82 disease modelling.

83

84 Here we hypothesised that it is possible to reproducibly generate functional brain organoids from retinal
85 confluent cultures of PSCs. We also asked the question if the retinal and brain organoids developing in
86 suspension culture together would form a complex retina-brain organoid system that would enable the
87 formation of an optic nerve-like structure.

88

89 We demonstrated here that the non-guided, simple and economical differentiation protocol, previously
90 described to spontaneously generate retinal vesicles from a confluent culture of hPSCs[19-21], also
91 generated brain organoids alongside the differentiation of retinal vesicles. The ease of precisely locating
92 cortical organoids, due to morphology and their proximity to retinal vesicles, reduced organoid variability.
93 Brain organoids were characterised as dorsal cortical organoids which, when further cultured in 3D
94 suspension, matured into functional organoids. A systematic comparison of scRNA-seq datasets
95 revealed a close similarity of our organoids with other dorsal patterned hPSC-derived brain organoids[16]
96 and proteomic analysis of late-stage organoids revealed the presence of numerous synaptic markers.
97 Organoids electrophysiological activity was dependent on organoids being cultured in relevant basal
98 medium[22] with proteomics providing insights into why this physiological environment aids

3

99 neurophysiological activity. Finally, the generation of retinal and cortical organoids facilitated the

100 isolation of both structures for 3D culturing, forming a complex organoid system. Notably, when cultured

101 in suspension, these retinal-brain organoids maintained the natural association created in the dish

102 during their spontaneous development which enabled the formation of optic nerve-like structures

103 between the two organoids.

104

105 **Results**

106 **Generation of self-forming retinal and dorsal cortical brain organoids from Confluent 2D/3D**

107 **cultures**

108 The retina is an extension of the CNS arising from the forebrain region in the developing embryo (**Figure**

109 **1a).** Indeed, the differentiation of whole brain cerebral organoids containing retinal structures has been

110 demonstrated[8,10]. **Figure 1b** schematic shows that proneural induction of confluent cultures of PSCs

111 spontaneously generate pigmented islands of retinal pigment epithelium (RPE) from which retinal

112 vesicles appear [19,21]. Further analysis of other structures forming in this 2D/3D environment highlighted

113 the presence of 3D regions containing clear neuronal rosettes forming in close proximity to retinal

114 vesicles. Based on the neuronal culture environment, and their morphological characteristics, we

115 hypothesised that these were brain vesicles. To fully characterise these structures, we manually excised

116 these regions to be grown in 3D suspension for maturation in culture, as previously described for their

117 retinal counterparts [21].

118

119 Following a neural induction period of 4-6 weeks in culture, neuroretinal vesicles and neural rosette

120 structures appeared (**Figure 1c**). These areas were manually dissected and grown in suspension in

121 retinal media from 7 weeks onwards to allow for maturation in a media composition previously described

122 in Lancaster et al., 2013 (**Figure 1d**). By 6 weeks of differentiation, 39% of all organoids observed in

123 cultures were retinal vesicles while 60% were neuronal organoids (n=10 2D/3D differentiation batches)

124 demonstrating that a proportion of cortical organoids are generated independently and are not in

125 proximity to retinal organoids. Immunohistochemistry (IHC) of 6-week old organoids revealed highly

126 proliferative KI67/NCAD positive neuroepithelium regions (**Figure 1e**). Active CASPASE3 cells were

127 also observed in the organoids. To mitigate this phenotype, organoids were further cultured on

128 previously-described shaking platforms (**Figure 1f**). Well-formed neuroepithelium regions contained

129 numerous SOX2/NCAD positive neural progenitor cells (**Figure 1g, h)** that were also immuno-positive

130 for cortical FOXG1 and NESTIN/PAX6 markers (**Figure 1j, S1a and SMovie 1**). These cortical

131 organoids were negative for ventral cortex specific marker, NKX2.1 (**Figure S1b**), as opposed to whole

132 brain cerebral organoids (**Figure S1c**), confirming the dorsal cortical origin of these organoids.

133   The presence of RPE and typical retinal vesicles facilitated the separation of dorsal cortical brain
134   organoids under bright-field microscopy from other forebrain-like neuroepithelia which also form in these
135   cultures (**Figure S1d-f**). These dorsal brain organoids could be easily distinguished in the 2D/3D
136   confluent cultures enabling the isolation of a population of dorsal cortical organoids for further maturation
137   and therefore minimising variability of mature cultures. We observed successful differentiation and these
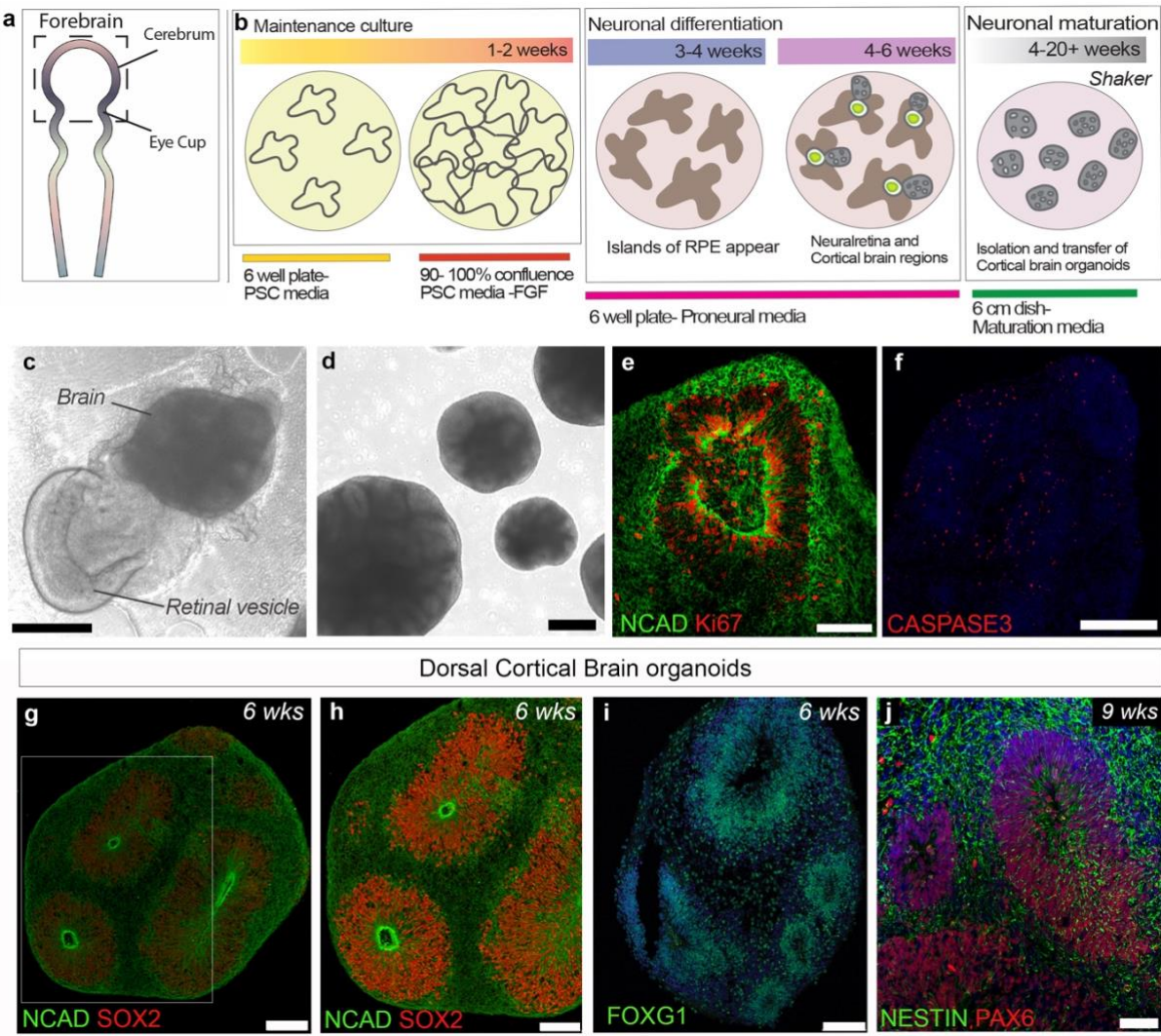138   culture features across a number of iPS stem cell lines (**Figure S2**).

Figure 1. Confluent PSC differentiation protocol gives rise to cortical and retinal organoids. a. Schematic illustrating neural tube formation and the formation of both cerebellum and eye cups from forebrain. **b.** Schematic summarising the 2D/3D differentiation protocol timeline for both retinal and cortical organoids formation as well as media composition and maturation in suspension. **c.** Representative image of a retinal vesicle and brain organoid in 2D culture. **d.** Bright-field image showing floating brain organoids, with typical neural rosettes, following manually excision from 2D culture. **e-j.** Immunohistochemistry images of 6 -9 weeks old brain organoids. **e, f.** Brain organoids showing Ki67 proliferative NCAD positive neuroepithelium and CASPASE 3 apoptotic cells. **g-j.** Cortical origin of brain organoids is confirmed by the presence of SOX2, FOXG1 and PAX6 positive neural precursors markers. Scale bars, 50 μm (j), 75 μm (h), 100 μm (e, g, i), 250 μm (f).

5

Cortical organoids differentiate into Cortical neurons and Glial cell types

Next, IHC confirmed the presence of cortical plate markers TBR1 which co-expressed with CTIP2-positive cells in the cortical organoids (**Figure 2a-c**). By 10 weeks of culture, CTIP2 regions also contained SATB2-positive cells (**Figure 2e, f**). From 8 to 12 weeks in culture, organoids increased in size significantly from 2000μm (± 560) to 2600μm (± 474) in diameter (**Figure 2g**, n=20-25 organoids, N=3 differentiation batches; mean ± SD, p=0.0002, unpaired two-tailed *t* test). This differentiation protocol also supported the differentiation of S100B- (**Figure 2g)** and GFAP-positive astrocytes that were present in similar percentages to TUJ1-positive neurons (**Figure 2h, i,** 75% (±14%) neurons versus 57% (±17%) glial cells; n = 10 images; N = 3-4 differentiation batches; mean ± SD, p <0.0001, unpaired two-tailed *t* test). Further IHC analysis at 15 weeks (~3.5 months) in culture demonstrated the presence of more mature inhibitory gamma aminobutyric acid (GABAergic) neurons (**Figure 2j, k** (high magnification of boxed area in A)) and their CALRETININ-positive subtypes (**Figure 2l**). Furthermore, 3D imaging of the whole-brain organoid by Lightsheet microscopy confirmed the presence of numerous inhibitory CALRETININ-positive neurons and GFAP-positive astroglial cell types (**SMovie 2**).
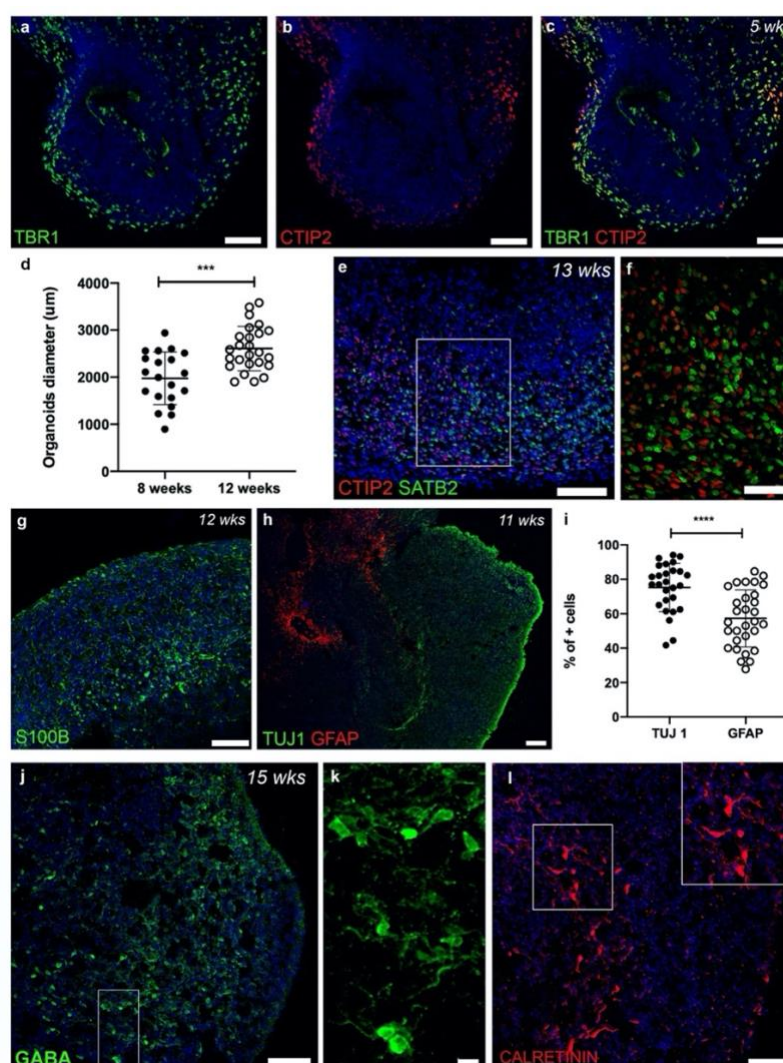

6

Figure 2. Cortical brain organoids generate cortical plate neurons and glial cells. a-c. Representative immunohistochemistry images of week 5 cortical organoids showing the presence of TBR1 and CTIP2 cortical plate neurons. **d.** Graph showing cortical organoids diameter and their significant size increase with days in culture (n= 30 organoids, N= 3 differentiation batches, mean ± SD, unpaired two-tailed *t* test). **e-h.** Representative images of organoids showing CTIP2 and SATB2 positive cells (**e, f**; high magnification image of inset in **e** shown in **f**) and S100B and GFAP glial cells (**g, h**). **i.** Graph showing the percentage of cells expressing TUJ1 and GFAP per area (mm2) in 11 weeks old cells. (n = 10 images from 2-3 organoids, N= 3 differentiation batches, mean ± SD, unpaired two-tailed *t* test). **j-l.** Week 15 cortical organoid showing GABA and CALRETININ positive inhibitory neurons, **k** shows high magnification image of inset in **j**. Scale bars, 15 μm (**k**), 50 μm (**f**), 75 μm (**a-c**), 100 μm (**e, g, h, j, l**).

Cortical Organoids from 2D/3D confluent cultures have similar cell type compositions to other brain organoids

Next, we performed scRNA-seq analysis using the 10X genomics platform to further investigate the cell-type composition of these dorsal cortical organoids and to establish their similarity to other published brain organoid scRNA-seq datasets, which were derived from various directed and undirected protocols. We used scClassify[23], a machine learning-based method, to annotate cell types that were present in our scRNA-seq cortical organoids (**Figure 3a**) and compared the composition of cell types in 3-month-old cortical organoid (CO) we generated against those from 3- and 6-month-old brain organoids and cell types from gestational week 12 (GW12) pre-frontal lobe (PFL) foetal brain (**Figure 3b**).

First, we compared the composition of cell types by using the cell type labels from the original authors for each of the published datasets, summarised in the table in **Figure 3b**. Although the proportions of each cell type varied across protocols, the overall cell type compositions were similar. This was independent of the protocol, their method of differentiation (directed or undirected) and age of the organoid (**Figure 3c**). In this analysis, Quadrato et al data (Quad 3M U) showed the most diverse cell-type composition.

Next, we utilised scClassify to annotate cells in our CO scRNA-seq dataset by training the classification model using either each individual public dataset as a reference or using all datasets jointly (refer to as joint training) (**Figure 3d**). The predicted cell-type composition in CO scRNA-seq data was plotted with respect to the training data, and, irrespective of the training dataset, a similar cell-type composition was observed in our COs (**Figure 3d**). In agreement with this, the expression profiles of key marker genes for each cell type population were also largely consistent, irrespective of the training dataset (**Figure S3).** BMP responsive cells, intermediate (bright orange) and proteoglycan-expressing cell types were absent from our dataset. Note that cells are annotated as "unassigned" when they could not be classified to any cell type. Cells are annotated as "intermediate" when they could not be classified to a specific cell type but an intermediate among multiple cell types. This intermediate population (denoted with "*")

7

205   is different from the intermediate cell type annotated in the training datasets (bright orange). Since the

206   scClassify jointly trained using multiple reference datasets reduces both unassigned and intermediate*

207   classification, the classification result from the jointly trained model was used in subsequent comparison.

208   Organoid cell types were clustered in a tSNE plot showing that cortical neurons were the most abundant

209   cell type (**Figure 3e**). We then measured the agreement between different cell-type compositions across

210   the multiple datasets using intraclass correlation (ICC) and visualised these results (**Figure 3f**). Three

211   major correlating groups were evident in relation to cell-type compositions: (1) Velasco *et al.*, 6 mo.,

212   directed (Vela 6m D); (2) Quadrato *et al.*, 3 mo., undirected (Quad 3m U) and; (3) the remaining

213   protocols, which included our 2D/3D COs. In accordance with **Figure 3c**, except for Quad 3m U, all 3m

214   organoids and the GW12 foetal sample cluster together, suggesting similar cell-type composition.

215   Notably, our organoids closely resemble the guided differentiation of dorsally patterned forebrain

216   organoids (Vela 3M D), known for their reproducibility[16]. Cell-type proportions were more diverse when

217   Quad 3m U was used as training data, suggesting a unique cell-type composition in this dataset. In fact,

218   Quad 3m U cell-type annotations clustered as a group with Vela 6m D separate from Trujillo *et al.*, 6

219   mo., directed (Truj 6m D) and the remaining 3 mo. organoids. Therefore, whilst cell-type composition of

220   Vela 6m D appeared to be different from those of 3m organoids, the composition of Truj 6m D was more

221   similar to 3m organoids. These results demonstrated the transcriptional similarities between cortical

222   organoids from spontaneous 2D/3D cultures and previous described brain organoids and the foetal
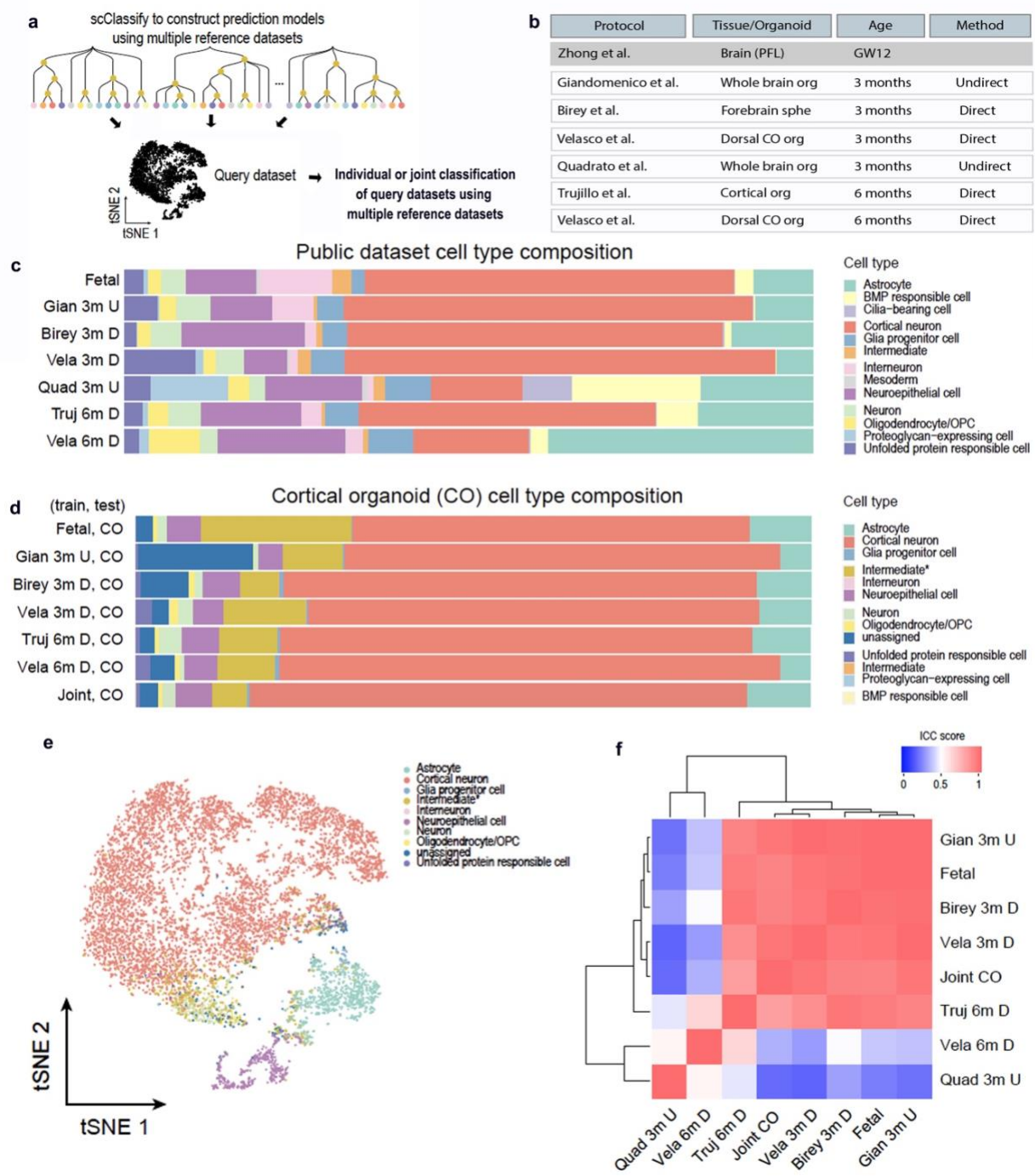
223   nervous system.

224

225

Figure 3. Comparison of cortical organoids and scRNA-seq available dataset. a. Schematic illustrating scClassify computational analysis to categorise a dataset using multiple reference datasets. **b.** Table summarising the public scRNA-seq reference datasets included in comparison and their differentiation protocols. **c.** Cell types composition in public datasets based on the annotation from their original studies. **d.** Cell-type composition in cortical organoids (CO) scRNA-seq dataset predicted by scClassify trained by each or all (i.e. Joint) public datasets. **e.** tSNE plot illustrating the cell types composition in CO based on scClassify annotation using Joint training. **f.** Interclass correlation heatmap showing the agreement between cell-type compositions among different organoids and a fetal brain.

Proteome analysis of brain organoids highlights increased abundance of proteins related to synaptic transmission

The proteomes of iPSCs and cortical organoids were surveyed to a depth of 6,244 and 5,719 proteins, respectively (after filtering and counting only unique genes). There were 4,444 proteins present shared between the iPSC and cortical organoid lists. Gene ontology enrichment analysis was performed with a focus on biological process and KEGG pathway terms (**Figure 4a-d**). **Figure 4a** shows the top thirty biological process terms that had the largest difference in significance between iPSCs and cortical organoids. Terms related to the cell cycle, chromosomes and DNA were more likely to be enriched for iPSCs, whereas terms related to the synapse, synaptic vesicles, vesical transport, axon/dendrite development and neuron projection were more enriched for cortical organoids. Since we are interested in neuronal differentiation in organoids, we extracted the top five synaptic and development terms (not already shown in **Figure 4a**) from the list of significant biological process terms (**Table S2**). For example, the terms "postsynapse organisation" and "regulation of postsynaptic membrane neurotransmitter receptor levels" were enriched for cortical organoids (**Figure 4b**). Neuron development and dendritic spine development were enriched for cortical organoids (**Figure 4c**). The KEGG pathway terms ribosome biogenesis in eukaryotes, DNA replication, cell cycle, and basal transcription factors were more enriched for iPSCs while axon guidance, neurotrophin signalling pathway and long-term potentiation terms were enriched for cortical organoids (**Figure 4d**). Examples of detected proteins that were exclusive to the iPSCs and are involved in stem cell proliferation and maintenance include proteins encoded by *LIN28A*, *BMPR1A*, *FGFR1*, *SOX2*, *ARID1A* and *RTF1* (**Figure 4e**). Conversely, GABA receptor subunits (encoded by *GABBR1* and *GABRG2*), a glutamate receptor subunit (encoded by *GRIA1*), a mediator of postsynaptic plasticity (encoded by *SYNGAP1*), a trans-synaptic protein (encoded by *NRXN1*) and two synaptic vesicle associated proteins (encoded by *SYN1* and *SYP*) are examples of proteins detected exclusively in cortical organoids (**Figure 4e**). The presence of these proteins and enrichment of relevant gene ontology terms confirms there was strong proteomic evidence that cortical organoids differentiated towards the neuronal- and away from a stem cell-phenotype.
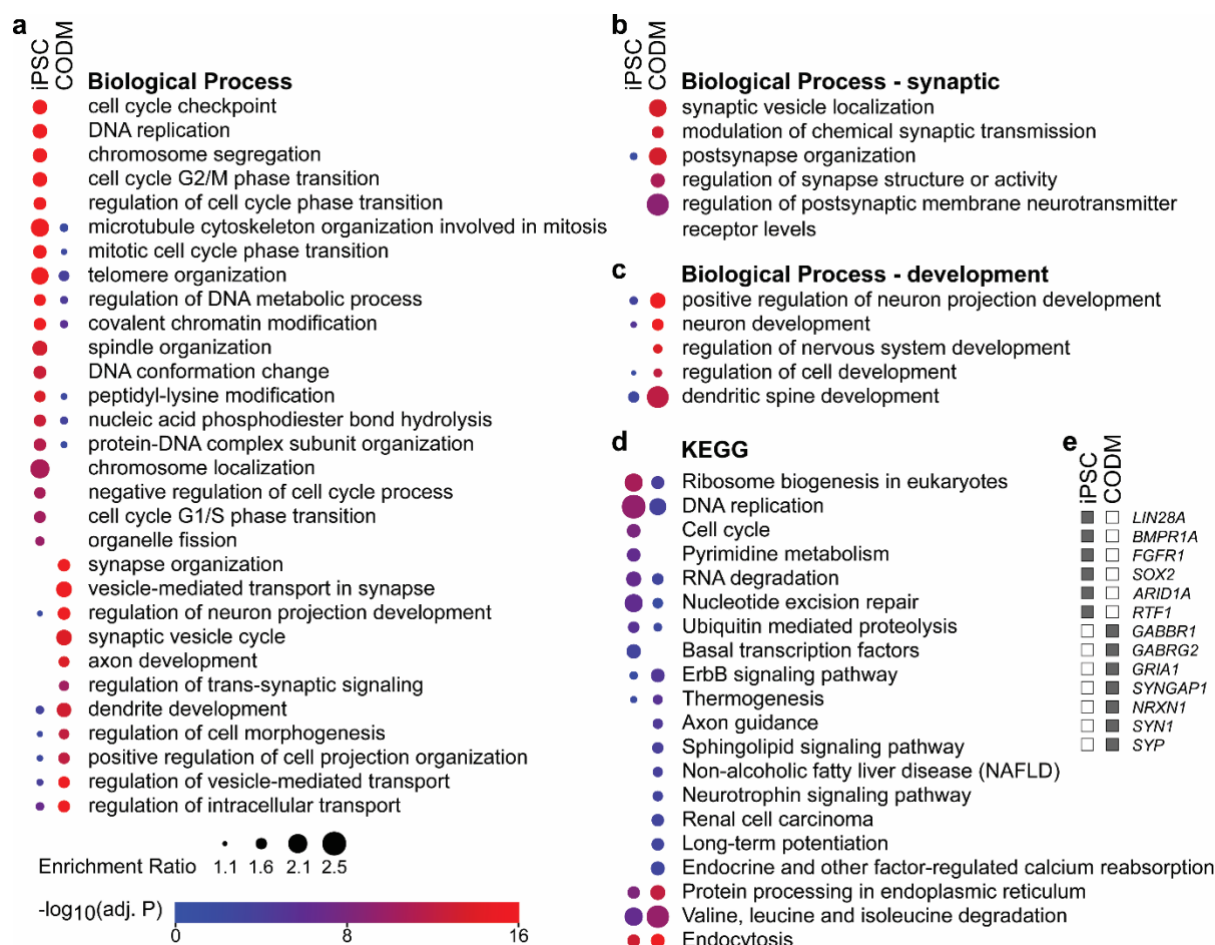
Figure 4. Comparison of the iPSC and cortical organoid proteomes using gene ontology enrichment analysis. a. Comparison of biological process terms with the largest difference in probability of enrichment for the genes encoding proteins detected in the iPSC and cortical organoid proteomes, the latter grown in cortical organoid differentiation medium (CODM). The colour scheme represents the value of $-\log_{10}(P)$, where P is the probability of enrichment adjusted by a false discovery rate of 5%. The size of each circle represents the ratio of enrichment. Absent circles indicate an enrichment ratio < 1.1. **b**. The top five biological process synaptic terms not already shown in **a**. **c**. The top five biological process development terms not already shown in **a**. **d**. Comparison of the KEGG pathway terms. **e**. Examples of proteins detected exclusively in either iPSCs or cortical organoids involved in maintenance of stems cells or synaptic functions.

2D/3D iPSC-derived Cortical Brain Organoids showed mature neuronal morphology and function.

Next, we sought to evaluate maturation and functionality of cortical organoids. Maturation of neurons is usually attributed to the presence of synapses. We first used IHC to examine synapse formation in organoids. MAP2 positive glutamatergic excitatory neurons expressing the vesicular glutamate transporter 1 (VGLUT1) protein were evident in brain organoids **(Figure 5a, b** (high magnification of boxed area in A)). Pre-synaptic protein synaptophysin was readily detected in puncta that localised in proximity to postsynaptic density protein PSD95 **(Figure 5c)**. Similarly, inhibitory GABA neurons and a

11

280   punctate pattern of presynaptic VGLUT1 were also evident in 2D cultures of dissociated of brain

281   organoids (**Figure S4**). To comprehensively characterise the synaptic machinery in these organoids we

282   analysed the proteome of 5 months-old organoids (n=3 organoids per batch, N=3 different batches of

283   differentiation): cell type specific enrichment confirmed the presence of all expected cell types including

284   neurons, astrocytes and oligodendrocytes. Finally, ultrastructure analysis by transmission electron

285   microscopy (TEM) demonstrated the presence of typical synaptic structures showing synaptic vesicles

286   and electron-dense synaptic contact sites (**Figure 5d, e**, asterisks and arrowheads, respectively).
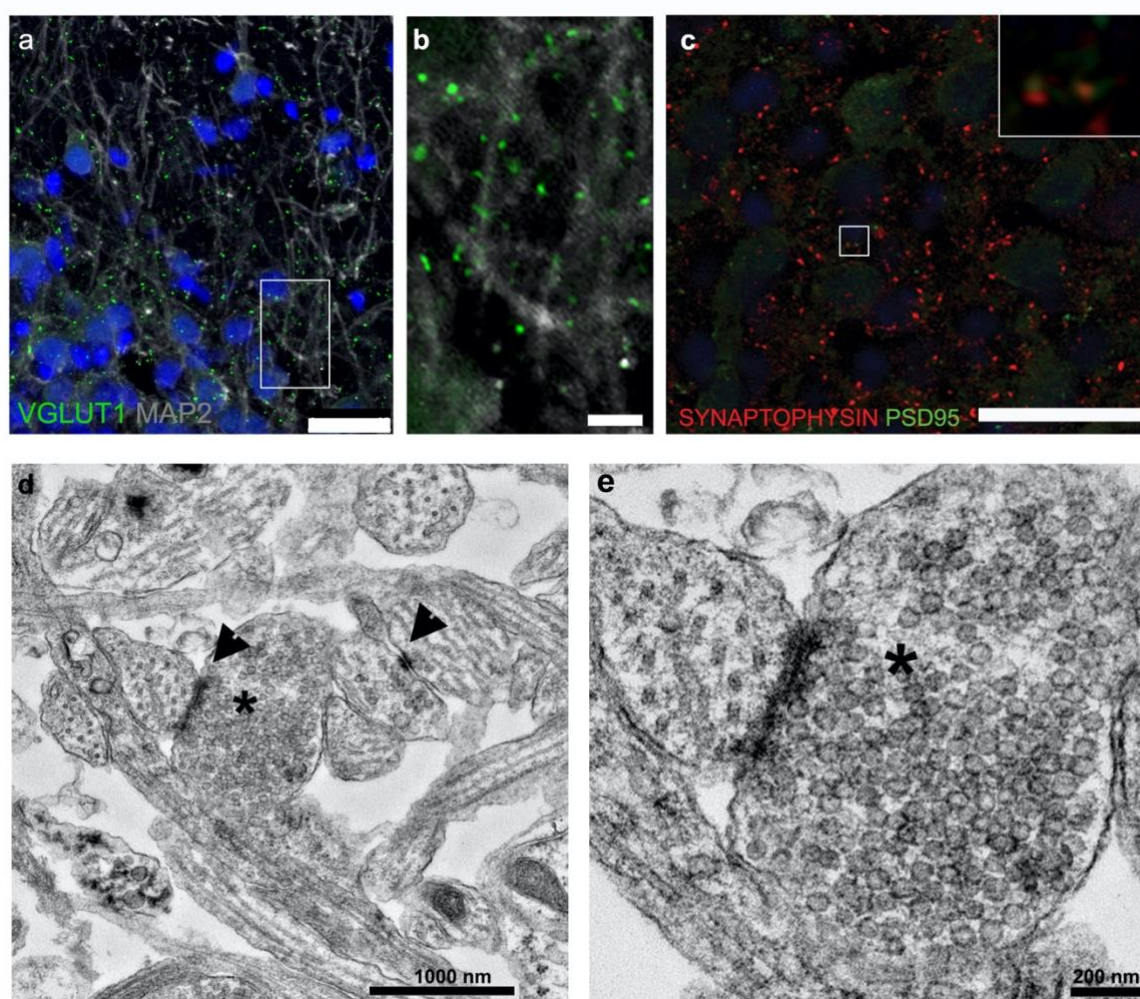
287

289   **Figure 5. Cortical organoids synaptic maturation**. **a, b.** Representative immunohistochemistry
290   images showing VGLUT1 puncta in MAP2 neuronal dendrites (**b**, high magnification image of inset in
291   **a**). **c.** SYNAPTOPHYSIN pre-synaptic and PSD95 post-synaptic synaptic markers. **d, e.** Ultrastructure
292   electron microscopy images of cortical organoids showing synaptic clefts (head arrows) and synaptic
293   vesicles (asterisks).   Scale bars, 5 μm (b), 25 μm (a, c).

294

295

12

296   We next tested the neurophysiological activity of organoids by multielectrode array (MEA). Five months-
297   old organoids were cultured in standard conditions until 2 months prior to recordings and then with either
298   cortical organoid differentiation medium (CODM) or a physiological relevant neuronal medium
299   (BrainPhys) up until the MEA recordings. Organoids were placed on the MEA one day before recordings
300   (**Figure 6a**). Spontaneous firing activity was observed in organoids cultured in BrainPhys (**Figure 6b,
301   c**), but not in CODM organoids. Similarly, spike raster plots showed firing patterns of organoids across
302   all electrodes with marked network bursts in organoids cultured in BrainPhys only (**Figure 6d, e and
303   S5a**). The mean firing rate (MFR) of neurons cultured in BrainPhys was significantly greater than CODM
304   grown organoids (1.7 ± 1.3 Hz in BrainPhys and 0.03 ± 0.04 Hz in CODM (n = 5 organoids, N=3
305   independent batches of differentiation, mean ± SD 60 electrodes, paired two tailed t-test, p= 0.0466)
306   (**Figure S5e**). Next, we performed pharmacological intervention using tetrodotoxin (TTX) as a synaptic
307   blocker. Organoid network activity was abolished with TTX addition with activity returning to normal
308   levels after washout (**Figure 6f**, n=5 organoids, N= 3 differentiation batches, mean ± SD, paired two
309   tailed t-test, **** p<0.0001).
310
311   BrainPhys medium has been described as a more physiological environment supporting the basic
312   function of neurons[22]. To gain insights into possible differences between BrainPhys and CODM cultured
313   organoids we compared the proteome of organoids cultured in the two media (**Figure 6g, h,** n= 3
314   organoids for each condition). Proteomic analysis detected 4,334 in common proteins for both conditions
315   with an additional 27 and 242 unique Brain Phys and CODM proteins, respectively. The different culture
316   conditions showed differences in protein enrichment (**Figure 6g**). Notably, enriched proteins that could
317   potentially explain the improved function of BrainPhys cultured neurons included synaptic vesicle-
318   associated proteins synaptophysin (encoded by *SYP*) and synaptotagmin 1 (encoded by *SYT1*),
319   glutamate receptor delta 1 subunit (encoded by *GRID1*) involved in synaptogenesis and phosphatase
320   and tensin homolog (encoded by *PTEN*) responsible for synapse maturation. Furthermore, organoids
321   were transduced with an AAV9.SYN1 (*Synapsin 1*) promoter driving an mcherry reporter Synapsin 1
322   tethers pools of synaptic vesicles in nerve terminals, binds to the cytoskeleton, and has an activity-
323   dependent function regulating the availability of synaptic vesicles for neurotransmitter release[24]. When
324   cultured in BrainPhys, organoids showed increased neuronal *Synapsin 1* promoter activity when
325   compared to standard CODM organoids (**Figure S5a, b**). We also confirmed the presence of synapses
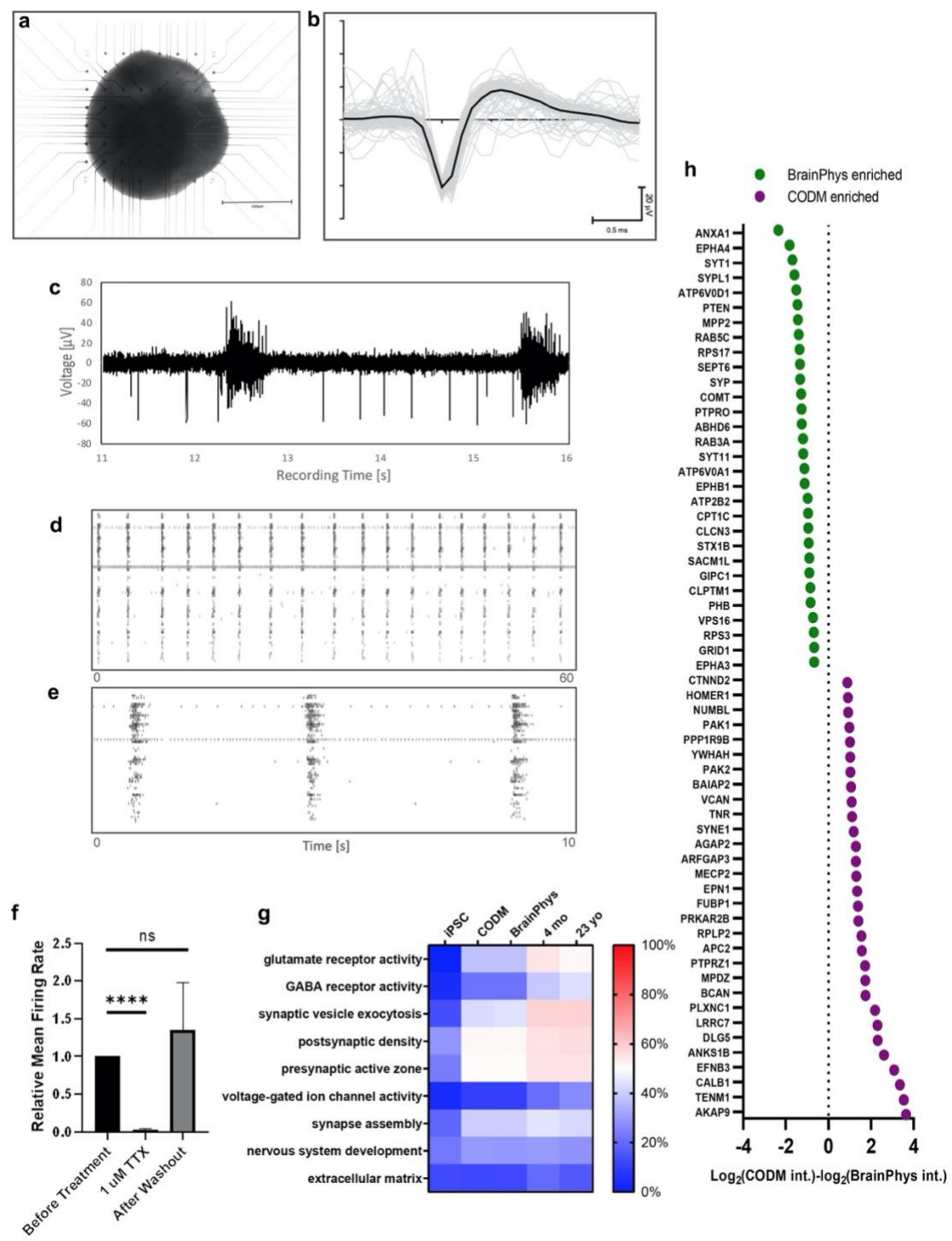326   and synaptic vesicles in BrainPhys organoids using TEM (**Figure S5f**).

Figure 6. Cortical organoids develop synchronous networks. a. Image showing cortical organoid plated overnight on Multielectrode array (MEA). **b, c.** Representative spontaneous firing activity of organoid. **d, e.** Spike raster plots showing firing patterns of organoids across all electrodes with marked network bursts. **f.** TTX treatment abolished firing activity, which returned following (mean ± SD, paired two tailed t test, **** p<0.0001). **g.** Graph showing proteins significantly differentially enriched in organoids cultured in CODM or BrainPhys media (p < 0.05, adjusted by a false discovery rate of 5%).

14

335 **3D retinal-cortical organoids form optic nerve-like structures**

336 Having demonstrated the formation of dorsal cortical organoids from 2D/3D confluent differentiation

337 cultures, we next aimed to test whether the 3D suspension culture of complex organoids comprising

338 both retinal and brain organoids promoted the formation of connections between the two organs.

339

340 In early 2D differentiation cultures, retinal and brain organoids spontaneously developed in proximity

341 enabling the manual isolation of these two organoids for further neural maturation in suspension (**Figure**

342 **7a**)**.** This differentiation potential was tested in 4 PSC lines (see Methods for details), including the

343 H9.mcherry embryonic stem cell (ESC) line where the typical morphology of brain neural rosettes and

344 thick neural epithelium of retinal organoids are easily discerned. At this early time point in 3D culture (5

345 weeks) the two organoids were attached but failed to show any clear axonal projections (**Figure 7b**)**.**

346 The connection of the retina to the brain to process the visual information is established by retinal

347 ganglion cells (RGCs), the first-born cell type of the retina, which form neuronal outputs connecting to

348 the brain through the optic nerve. In the complex retinal-brain organoids, at 10 weeks of development,

349 the maturation of each individual organoid was evident. In retinal organoids NEUN and HuC/HuD

350 colocalised with THY1 and MAP2 RGC markers delineating these cells' axonal projections towards the

351 centre of the organoid (**Figure S6a, b**). Similarly, these two markers were also expressed in neurons

352 within the brain organoids, as demonstrated by the colocalization with TBR1 cortical neural marker

353 (**Figure S6c, d**). CRX positive photoreceptor cells were present in retinal organoids with RGC THY1

354 positive axons clearly extending long axonal processes that connect to the TBR1 positive brain organoid

355 (**Figure 6c, d,** n= 13 organoids, N= 9 differentiation batches)**.** Finally, we used Lightsheet microscopy

356 to image the morphological intricacies of whole 3D retinal-brain complex organoids (n=3 organoids, N=2

357 differentiation batches). Cleared organoids enabled the visualisation of MAP2 positive projections

358 connecting both retinal and brain regions forming structures that resemble the optic nerve (**Figure 7e,**
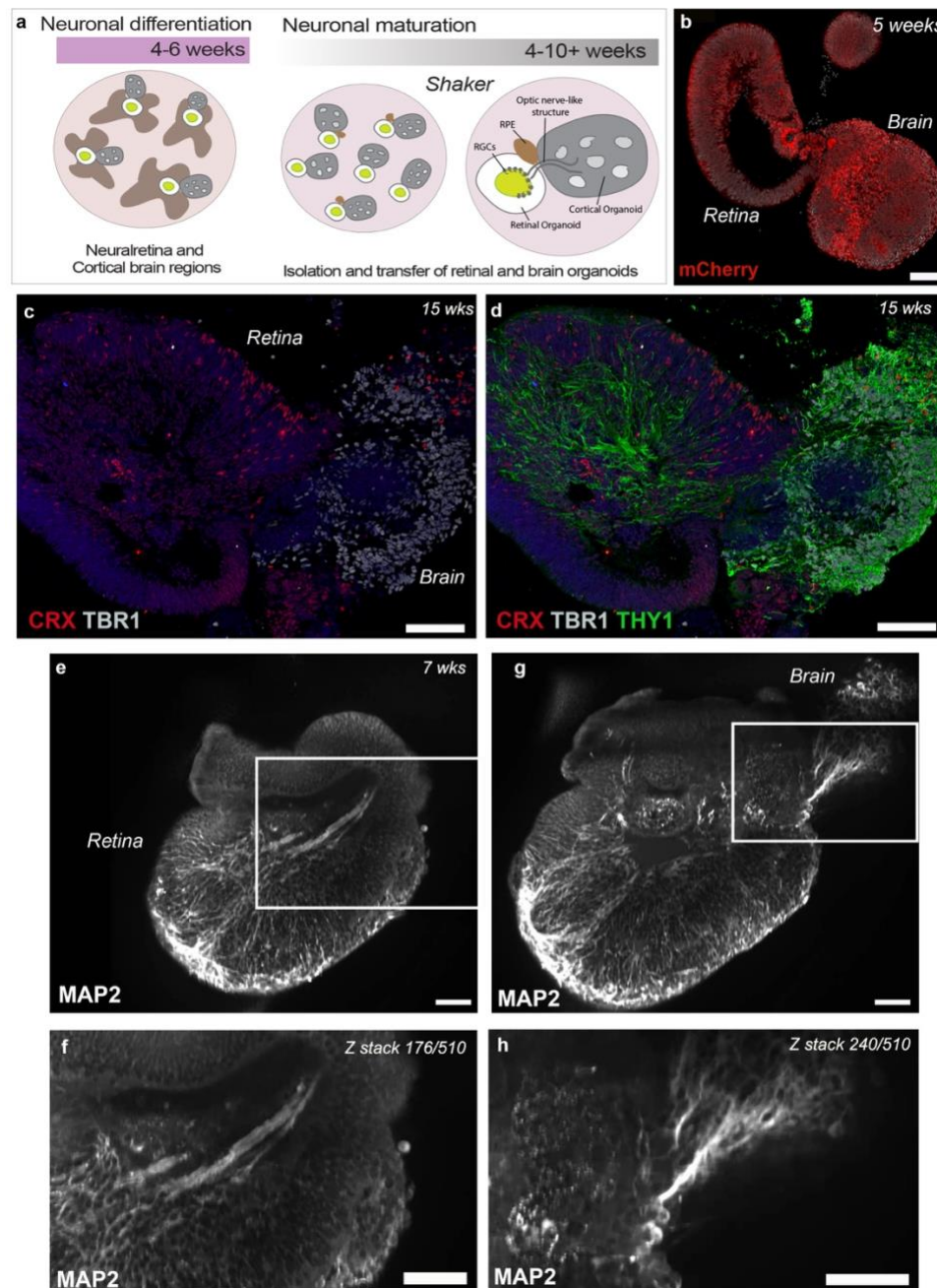
359 **h and SMovie 3,** n=3 organoids imaged).

Figure 7. Complex retinal-cortical organoids form optic nerve-like structures. a. Schematic illustrating the timeline of neuronal differentiation and the main cellular components of the retinal-cortical system. **b.** Week 5 mCherry retinal-brain organoid showing retinal and brain regions growing together. **c.** Representative immunohistochemistry images of CRX positive photoreceptor cells in retinal organoids and TBR1 neurons in brain organoids. **d.** THY1 positive retinal ganglion cells send axonal projections to the centre of the retinal organoid that connect with brain organoid THY1 positive neurons in brain regions. **e-h.** Light sheet image of whole retinal-brain organoid showing consecutive z-stack images of MAP2 retinal ganglion cells axons. **e.** Forming optic nerve-like structure projecting towards the central part of retinal organoid (**e**). **f.** High magnification image optic nerve-like structure (z stack 176 out of 510 stacks) from inset in **g**. Deeper z-stack 240 showing the same axonal projection connecting to brain region. **h.** High magnification image of inset in **g** showing optic nerve-like structure. Scale bars, 100 μm (b-d), 200 μm (e-h).

Discussion

373
374
375   The differentiation of PSCs into retinal and brain organoids have been used to model several
376   neurodegenerations. A fundamental requirement for the development of therapies is the establishment
377   of robust pre-clinical models in which they can be tested. Whilst numerous retinal and brain organoid
378   differentiation protocols have been described, these differ considerably in methodology: some methods
379   rely entirely on the addition of growth factors and matrices to guide cell fate decisions and organ
380   formation while others form spontaneous organoids through the endogenous potential of PSCs to form
381   the niches of miniaturized organs *in vitro*. Variability between protocols and, most importantly, in-batch
382   organoid variability is a common problem of both approaches. Other challenges include the phenotypical
383   and maturity differences between *in vitro* generated cells and their *in vivo* counterparts. Furthermore,
384   the generation of the right cell type to enable the robust analysis of functional assays and testing of new
385   therapies requires long-term cultures. Each of these protocols present their own advantages and
386   disadvantages. However, to facilitate scale up and the high throughput use of these brain-like models,
387   their variability and culture costing are usually the most common challenges and, thus, the initial choice
388   of protocol is important.

389

390   Here, we adapted a previously-described simple and robust 2D/3D differentiation approach derived from
391   confluent cultures of PSCs[19] and generated dorsal cortical organoids within the same cultures of retinal
392   vesicles and RPE cells. These cortical organoids are morphologically different and distinguishable from
393   retinal vesicles which display thick neuroephithelia. Instead, brain organoids form the neural rosettes
394   typical of cortical organoids, a feature that enabled their ready isolation. This differentiation method only
395   requires a confluent culture of PSCs followed by change to a pro-neural induction media. Particularly
396   important to reducing variability and costs of long-term cultures, this simple method does not require the
397   addition of Matrigel or exogenous factors. Having tested this protocol in various PSC lines, we confirmed
398   the generation of dorsal cortical organoids that express typical cortical plate markers as well as inhibitory
399   and excitatory neurons and glial populations, with very few PSC lines failing to give rise to neuronal
400   tissues.

401

402   The initial extracellular matrix and local cell-cell interactions provided by the 2D confluent environment
403   of differentiating PSCs is sufficient to drive self-formation of discrete 3D structures, such as the eye and
404   the brain. PSC cell lines vary in their efficiency to specify towards the three embryonic germ layers due
405   to cell intrinsic cues specific to each cell line. Self-forming spontaneous methods benefit from the default
406   bias present in most PSC lines to form ectoderm and forebrain[25]. Omics analysis of PSC lines and their
407   initial stage of differentiation have shed light on the variability between cell lines leading to increased

17

408 differences between organoids generated among multiple cell lines[10,26]. Our undirected protocol enables

409 reproducibility of directed organoids but with the benefits of spontaneous differentiations.

410

411 Despite tremendous progress in the field, the lack of disease-relevant functional assays in organoids

412 hinders their ability to test for new treatment efficacy. However, disease molecular signatures and

413 biomarkers can be determined using integrative analysis of omics as well as computational or

414 bioinformatic methodologies. In this study, cortical organoids generated by 2D/3D confluent method

415 were extensively characterized using scRNA-seq and proteomics analysis, setting a baseline for future

416 studies using disease organoids. In agreement with a previous correlation study comparing scRNA-seq

417 datasets of brain organoids and foetal human brain[12], our organoids showed a high correlation with brain

418 organoids derived by other methodologies, particularly with dorsally patterned brain organoids

419 generated in the directed differentiation approach demonstrated in Velasco et al., 2019[16], known for

420 their reproducibility.

421

422 The proteome of brain organoids has been seldom investigated. Previous proteomic analysis of early-

423 staged (day 45) brain organoids generated using a whole-brain spontaneous 3D aggregation method

424 highlighted the protein–protein interactions involved in early neuronal specification, including the

425 migration of progenitor cells, radial glia, and oligodendrocyte progenitors[27]. Our proteomic analysis

426 compared iPSCs and five months old cortical organoids. The analysis supported the increase in

427 expression of proteins related to neuronal development and synaptic function in the cortical organoids

428 and a relative decrease in cell cycle related proteins. The detection of synaptic protein components was

429 further corroborated by IHC for synaptic markers and ultrastructure electron microscopy.

430

431 Neuronal network formation in brain organoids have previously been studied elegantly in late-stage

432 organoids cultured on the MEA for a few months[10,15] and in bioengineered neuronal organoids[28]. Our

433 own electrophysiology analysis verified the functionality of cortical organoids, demonstrating their

434 synchronous neuronal network activity when cultured for the final two months of differentiation in an

435 electrophysiologically-relevant medium, BrainPhys[22]. A separate proteomics analysis identified proteins

436 enriched in the BrainPhys-cultured organoids that might explain how BrainPhys media promotes

437 favourable protein expression and electrophysiological activity. Overall, these results demonstrate the

438 generation of functional cortical organoids that can be reliably differentiated for disease modelling and

439 precision medicine studies.

440

441 Neurodevelopmental disorders leading to higher order cognitive abilities mostly affect the cortex and

442 thus modelling of these conditions using cortical organoids is crucial[29]. In the eye, numerous retinal

18

443   diseases have been investigated using retinal organoids[30,31-38]. However, modelling of more complex

444   disease traits requires the differentiation of specific brain regions and their functional integration as well

445   as their connection with other organs. One example of complex organotypic formation was

446   demonstrated by the fusion of cortical, spinal cord organoids and skeletal muscle spheroids which

447   generated a functional cortico-motor assembloid system leading to robust muscle contraction[39].

448

449   In this study, we demonstrated the spontaneous formation of retinal-and-brain complex organoids in the

450   2D/3D confluent cultures. When in 3D suspension, these retinal-brain organoids maintained their

451   proximity and were connected through an optic nerve-like structure mimicking the neuronal projections

452   that connect the eye and brain. Our confluent method of differentiation enabled the precise isolation of

453   these two organoids, overcoming variability within 3D directed and whole brain protocols that

454   sporadically generate eye structures[8,10] and the forced fusion of different organoids to form assembloids.

455   The latter have been successfully used to model *in vivo* neuronal interactions between different brain

456   regions[1,39-42]. The formation of optic nerve structures *in vitro* in complex organoid structures will better

457   elucidate the dynamics of retinogenesis and neurogenesis that can then be used to model a number of

458   optic neuropathies, such as glaucoma. Importantly, these retinal-brain organoids also promise to

459   improve organoid development, such as the long-term survival and maturation of retinal ganglion cells

460   in the retinal organoids as these cells would no longer lack their contact with the output in the cortex.

461   Neurodegeneration in glaucoma is complex and extends beyond the eye into the lateral geniculate

462   nucleus and visual cortex[18] of the brain. Similarly, late onset neurodegenerative diseases, such

463   Alzheimer's show early phenotypes in the eye[17], which enables pre-symptomatic diagnosis[43]. Accurate

464   and more complex models of such diseases will elucidate novel aspects of disease pathogenesis and

465   aid the challenges of developing effective treatments.

466

467   Our data demonstrate the simple and undirected derivation of both cortical and retinal organoids from a

468   confluent culture of PSCs. The simplicity of this differentiation method coupled with the ease of precisely

469   locating dorsal cortical organoids, due to their proximity to retinal vesicles, addresses the current

470   problems of in-batch organoid-to-organoid variability. The comprehensive characterisation shown here,

471   including novel proteome data of brain organoids, expands the available repertoire of relevant models

472   of human disease. Importantly, this method also enabled the formation of complex organoid-forming

473   structures that resemble the important connection, between the retina and the brain, the optic nerve.

474   Future investigations of these neuronal populations and projections will allow the study of common optic

475   nerve neuropathies.

476

477

478   **Materials and Methods**
479

480   ***Derivation of UCLOOi017-A-1 induced pluripotent stem cell (iPSC) line***

481   Peripheral blood mononuclear cells (PBMCs) were isolated from the whole blood of a healthy donor

482   using density gradient centrifugation. Briefly, 25ml of whole blood diluted 1:1 with phosphate buffered

483   saline (PBS) was layered on top of 15ml of Ficoll-Paque Premium (GE) and centrifuged with brake and

484   accelerator off at 500g for 30 minutes and the cloudy interphase containing PBMCs was collected. After

485   washing once with PBS, the cells were counted and 2 million were cultured for 6 days in hematopoietic

486   expansion media -Stemspan H3000(Stemcell Technologies), with the addition of EPO (R&D), IL-3 (Life

487   Technologies), Dexamethasone (Sigma), Ascorbic Acid (Sigma), SCF (Miltenyi) and IGF-1 (Miltenyi).

488   Following expansion, 200000 cells were nucleofected using Amaxa 4D nucleofector with Addgene

489   plasmids   pCXLE-hUL   (Addgene   plasmid   #27080;   http://n2t.net/addgene:27080;

490   RRID:Addgene_27080), pCXLE-hSK (Addgene plasmid #27078; http://n2t.net/addgene:27078;

491   RRID:Addgene_27078)   and   pCXLE-hOCT3/4-shp53-F   (Addgene   plasmid   #27077;

492   http://n2t.net/addgene:27077; RRID:Addgene_27077) [pCXLE-hUL, pCXLE-hSK and pCXLE-

493   hOCT3/4-shp53-F were gifts from Shinya Yamanaka]. The nucleofected cells were plated on a well of

494   a 6 well plate coated with Geltrex matrix (Life Technologies) and transitioned to Essential 8 media (Life

495   Technologies)[1]. iPS cells were visible within a week and small colonies were visible within 2 weeks.

496   Four to five weeks later, iPSC colonies were large enough to be excised, broken up and transferred

497   using a 10µl pipette to individual wells of a 12 well plate (Corning). Once colonies had enlarged in the

498   12 well plate, each well (containing an iPSC clone) was dissociated and further cultured separately on

499   6 well plates (Corning) for 10 passages prior to characterisation.

500

501   ***Human PSC maintenance***

502   The human pluripotent stem cells including iPSC (UCLOOi017-A-1, ECCACs HPSI0214i-kucg_2 and

503   HPSI0314i-hoik_1 and TiPSC-5[2]) and ESC (WiCell H9 WA09, H7 WA07) lines were maintained on

504   feeder free conditions on Essential 8 media (E8, Life technologies) and Geltrex (Life technologies)

505   coated 6 well plates. Briefly, when 70% confluent, PSCs were dissociated using Versene solution (Life

506   technologies) at 37°C for 5 to 10 minutes. The dissociated clumps were washed once in PBS with

507   centrifugation at 900 rpm for 5 minutes. The resulting cell pellet was broken up and resuspended in 1ml

508   E8 media by 1000ul pipette and distributed on a Geltrex coated 6 well plate with E8 and 10µM ROCK

509   inhibitor (Y-27632 dihydrochloride, Tocris) for 24 hours. Daily feeding with E8 was continued for further

510   maintenance culture.

511

512   ***Differentiation of PSC into cortical organoids***

513   Human iPSCs were maintained until 90-95% confluent as described above. Media was replaced with
514   Essential 6 media (E6, Life Technologies) for 2 consecutive days. At day 3 of differentiation, E6 media
515   was replaced with a pro-neural induction media (PIM, composed of Advanced DMEM/F12, N2
516   supplement, L-Glutamine, non-essential amino acids and Antibiotic-antimycotic). At around week 3-4
517   of culture, three-dimensional (3D) organoids containing rosettes were observed throughout the plate
518   and in close proximity to neuroretinal vesicles. The 3D cortical organoids were manually excised with
519   19G needles and kept together in 60 mm well plates in retinal differentiation media (RDM, composed of
520   DMEM, F12 Nutrient mix, B27-vitamin A and antibiotic-antimycotic) and placed on an orbital shaker at
521   85 RPM. At 6 weeks of differentiation, retinal differentiation medium was supplemented with 10 % FBS,
522   100 µM Taurine (Sigma, T4871) and 2 mM Glutamax. At 10 weeks, cortical organoids were cultured in
523   a cerebral organoid differentiation medium (CODM) as described in Lancaster & Knoblich, Nature
524   Protocols, 2015 (Composed of Neurobasal medium, DMEM/F12, N2 supplement, insulin, Glutamax,
525   MEM-NEAA, B-mercaptoethanol, B27 supplement) or BrainPhys^{TM} hPSC Neuron Kit (Stemcell
526   Technologies, composed of BrainPhys Neuronal medium, NeuroCult SM1 neuronal supplement, N2
527   supplement, human recombinant brain-derived neurotrophic factor, human recombinant glial cell line-
528   derived neurotrophic factor, ascorbic acid and dibutyryl-cAMP). Differentiation cultures were fed every
529   Monday, Wednesday and Friday. All representative images in the paper were from ***UCLOOi017-A-1***
530   iPSC line unless otherwise stated.
531

Immunohistochemistry

533   hPSC-derived Cortical organoids were used for assessments of the time course of differentiation, as
534   described in the main manuscript. Cortical Brain Organoids were washed with PBS, fixed for 40 minutes
535   to 60 minutes depending on the size of the organoid in 4% paraformaldehyde and washed again with
536   PBS prior to overnight suspension in 20% sucrose. The organoids, once sunken in sucrose, were
537   embedded in OCT and snap frozen in nitrogen.
538   Cortical brain organoids were cryo-sectioned at 14 um thickness, collected on SuperFrost slides
539   (Thermo) and preserved at minus 20°C. Cryosections were washed with PBS and blocked in 5% serum
540   (goat or donkey) in blocking solution (1% Bovine serum albumin in PBS with 0.1% Triton-X) for 2 hours.
541   Primary antibody (**Supplemental Table 1**) diluted in blocking solution was incubated overnight at 4°C.
542   Sections were washed with PBS three times and incubated with secondary antibody (Alexa fluor 488,
543   546, 633 secondary antibodies, Invitrogen-Molecular Probes) diluted in blocking solution (1:500) at room
544   temperature. Sections were then washed with PBS and counter stained with DAPI (Sigma-Aldrich).
545   For immunohistochemistry of whole cortical organoids in 3D view using Lightsheet, a clearing protocol
546   was performed. Briefly, cortical brain organoids were fixed in 4% paraformaldehyde, suspended in 20%
547   sucrose and stored in 4°C as described above. Samples were incubated in clearing reagent 1 (Urea,

548   N,N,N',N'-tetrakis, Triton X, NaCl, dH_2O) overnight followed by block in blocking solution (1% BSA in

549   PBS, 5% serum and 0.3% Triton X) for 2 hours or overnight. Primary antibodies and DAPI were added

550   in the blocking solution without serum overnight to increase penetration of antibody. Samples were

551   washed with PBS and secondary antibodies diluted in blocking solution at 1:500 were added to the

552   organoids overnight. The following day, samples were washed with PBS and clearing reagent 2

553   (Sucrose, Urea, Triethanolamine, Triton X, dH_2O) was added overnight. Samples were embedded in

554   low melting point agarose and left hanging in clearing reagent 2 for approximately 1 or 2 days until the

555   samples were clear.

556

Image acquisition

558   Images were acquired by confocal microscopy (LSM 880 Airyscan or SP5 Leica). A series of XY optical

559   sections, approximately 1.0μm apart, throughout the depth of the section were taken and built into a

560   stack to give a projection image. For Zeiss and Leica, ZEN blue and LAS AF image software were used,

561   respectively. For Lightsheet fluorescence microscopy, images were acquired using Zeiss Lightsheet Z.1

562   using similar parameters to normal confocal using Zen Black software. Further image processing was

563   performed in Imaris (version 9, Bitplane AG, Switzerland) software. Briefly, after images were imported,

564   surfaces for each of the channels were created using the Surface Creation Wizard. Smoothing and

565   threshold limits were applied to eliminate background light form the image. Optical sections of the

566   organoid were created using the Oblique Slicer tool.

567

Dissociation of Brain organoids

569   To produce 2D neuron cultures, cortical organoids were washed with PBS once and incubated in trypsin

570   or Accutase for 5 minutes at 37°C. Organoids were then dissociated into single cells by gently pipetting

571   up and down. Cells were then centrifuged at 300 *g* for 5 minutes and cell pellets were resuspended in

572   250 μl of media and seeded onto Geltrex coated 8 well chamber slides. Media was changed every other

573   day until dissociated cells reached 11 weeks in culture.

574   For scRNA-seq, cortical organoids were dissociated with Neurosphere dissociation kit (Miltenyi Biotec).

575   Cortical organoids were transferred to Eppendorf tubes then washed with 1 ml of PBS. Enzyme mix was

576   prepared as per manufacture instructions and 500 ul added to each tube and incubated at 37°C for 10

577   minutes and flicked every 2 minutes. Organoids were then pipetted up and down with p1000 pipette to

578   mechanically dissociate the big clumps of cells. The tubes were returned to 37°C for another 5 minutes

579   and further dissociation. Following this incubation, a p200 pipette was used to break up the clumps

580   further and 500 μl of HBSS was added to each tube and the contents were filtered using MACS 30 um

581   filters into fresh Eppendorf tubes. Cells were pelleted by centrifugation at 400 *g* for 10 minutes at room

582 temperature and resuspended in 200 µl of CODM media with the tubes kept on ice when transferred for
583 cell counting.

584

585 ***Quantification***

586 Chamber slides were fixed by incubating in 4% PFA for 10 minutes and stained with TUJ1 and GFAP
587 antibodies using the immunohistochemistry protocol described above. Next, cells were imaged using
588 the Zeiss Axio Imager Alpha confocal microscope. Cell clumps cells were located using epifluorescence
589 illumination and TUJ1 and GFAP positive cells were imaged from 10 different regions in the chamber
590 slide and quantified using FiJi software. To accurately measure the percentage of TUJ1 neurons and
591 GFAP glial cells, the number of DAPI, TUJ1 and GFAP cells were counted using cell counter plug-in.
592 Then the percentages of TUJ1 and GFAP cells were calculated by in relation to the total number of
593 DAPI cells.

594

595 ***Single Cell RNA-Sequencing***

596 Organoids were dissociated as described above and a subset of cell suspension was stained with 0.4%
597 Trypan Blue (Gibco) and assessed for viability and concentration using Countess II Automated Cell
598 Counter (Invitrogen). Single cell suspensions were passed through 40µm cell strainer (Corning) and
599 concentration was adjusted to 1000 cells/µl. The suspension was loaded in single-cell-B Chip (10X
600 Genomics) for target output of 10,000 cells per sample. Single-cell droplet capture was performed on
601 the Chromium Controller (10X Genomics). cDNA library preparation was performed in accordance with
602 the Single-Cell 3' v3 protocol. Libraries were evaluated for fragment size and concentration using Agilent
603 HSD5000 ScreenTape System. Samples were sequenced on an Illumina NovaSeq6000 instrument
604 according to manufacturer's instructions (Illumina). Sequencing was carried out using 2x150 paired-end
605 (PE) configuration with a sequencing depth of 40,000 reads per cell. The sequences were processed
606 by GENEWIZ. The data supporting the findings in this publication have been deposited in NCBI's Gene
607 Expression Omnibus and are accessible through GEO Series accession number GSE174232
608 (https://www.ncbi.nlm.nih.gov/geo/query/acc.cgi?acc=GSE174232).

609

610 ***Single Cell RNA Sequencing analysis***

611 Raw files were processed with Cell Ranger 2.0.1 software (10X Genomics). The Cell Ranger count
612 module was used to align sequence reads from scRNA-seq experiment to the GRCh38 human
613 reference genome and to generate the cell-by-gene count matrix. Genes and cells were filtered retaining
614 those that are expressed in at least three cells and those that have at least 500 genes detected. Cells
615 were further filtered by removing (i) those that have over 10 percent mitochondrial genes in all detected
616 genes and (ii) predicted doublets using DoubletFinder (Version 2.0.3)[3] with an expected rate of 2.5%

23

617 (according to 10X Genomics guidelines). To compare our cortical organoid scRNA-seq data with other

618 published datasets, a combined cell-by-gene count matrix of the processed scRNA-seq datasets with

619 cell annotation was obtained from OrganoidAtlas (https://cells-test.gi.ucsc.edu/?ds=organoidatlas)[4]. We

620 subset six scRNA-seq datasets from six different brain organoid studies each using a different

621 culture/differentiation protocol. These include Giandomenico et al., 2019 (denoted as "Gian 3m U"),

622 Birey et al., 2017[5] (Birey 3m D), Velasco et al., 2019[6] (Vela 3m D), Quadrato et al., 2017[7] (Quad 3m U),

623 Trujillo et al., 2019[8] (Truj 6m D), and Velasco et al., 2019[6] (Vela 6m D). A fetal brain dataset is also

624 included for comparison (Zhong et al., 2018)[9] (Fetal). The cell type compositions of each public dataset

625 were visualized as staked bar plots. Cell annotation of the cortical organoid scRNA-seq generated in

626 this study was carried out by using scClassify (Version 1.0.0)[10]. Briefly, we trained prediction models

627 using each published dataset as reference separately and joint trained. Then, we predicted the cell types

628 in our cortical organoid scRNA-seq based on the individual and the joint prediction models. A t-

629 distributed stochastic neighbour embedding (t-SNE) was applied to visualize the cells with labels

630 generated from the joint prediction model. To compare agreement in cell-type composition between our

631 cortical organoid and the public brain organoid and fetal brain datasets, intraclass correlation coefficient

632 (ICC) was calculated by generating a table of cell-type composition across published organoids and our

633 organoid, using the ICC function in the irr R package (Version 0.84.1). To evaluate the reproducibility of

634 cell type prediction, logarithm transformed data were used for assessing the expression of a panel of

635 marker genes listed in[4] in each cell type based on the scClassify prediction. The marker genes include

636 neuronal growth cone markers (STMN2, GAP43, DCX), early neurogenesis markers (VIM, HES1,

637 SOX2), excitatory neuron markers (TBR1, SLC17A7), inhibitory neuron markers (GAD1, SLC32A1),

638 radial glial marker (EOMES), cell cycle markers (TOP2A, MKI67), oligodendrocyte precursor cells

639 markers (OLIG1, OLIG2), astrocyte markers (S100B, SLC1A3, GFAP), cilium markers (MNS1, NPHP1),

640 BMP signal markers (BMP4, MSX1), mesoderm marker (MYH3), proteoglycan markers (BGN, DCN)

641 and   unfolded   protein   response   cell   marker   (DDIT3).

642

643 ***Electron microscopy (EM)***

644 Brain organoids were fixed overnight in Karnovsky's fixative (2.5% glutaraldehyde and 2.4%

645 formaldehyde in MOPS buffer), then washed in MOPs buffer. They were post fixed with 2% osmium

646 tetroxide, incubated in 2% aqueous uranyl acetate, dehydrated in an ethanol series, and embedded in

647 TAAB Low Viscosity Resin (TAAB Laboratories). Sections were cut at 90nm using a UC6 ultramicrotome

648 (Leica Microsystems), then stained with 2% uranyl acetate in 50% ethanol (10 min) and Reynold's lead

649 citrate (4 min). Grids were examined with a JEOL JEM-1400 transmission electron microscope operating

650 at 80 kV, with images recorded using a Matataki Flash sCMOS camera.

651

652 ***Recording of organoid activity on Multiple Electrode Array (MEA)***

653 After media replacement as described previously, a single organoid for each recording was placed onto

654 a 60-electrode MEA200/30iR-Ti multiple electrode array (MEA) plate (MultiChannel Systems), ensuring

655 coverage of the electrodes. Medium was removed and 20 µl of Matrigel extracellular matrix (Corning)

656 was dropped onto the organoid. The MEA plate was subsequently incubated at 37 °C for 15 mins to

657 allow the Matrigel to set the organoid in place. 500 µl of medium was added dropwise and the plate was

658 placed back in the incubator at [37 °C, 5% CO2, 70% humidity] for 24 hours before recording electrical

659 activity.

660 Organoid electrical activity was measured using an MEA2100-lite system with TC01 temperature control

661 (MultiChannel Systems), heated to 37 °C. Recordings were made for 5-10 minutes at a frequency of 10

662 kHz using MultiChannel Experimenter software (MultiChannel Systems). Data was processed using the

663 MultiChannel Analyzer software (MultiChannel Systems). Raw electrode recordings were filtered

664 sequentially with a 200 Hz second order Butterworth high pass filter then a 3 kHz second order

665 Butterworth low pass filter. Spikes were picked using a threshold of 5 standard deviations below mean

666 voltage for each electrode.

667 Voltage-gated sodium channel activity was blocked using Tetrodotoxin (TTX). Briefly, baseline activity

668 was recorded by MEA as described above. Immediately afterwards, Brainphys media was removed,

669 and washed once with PBS, then replaced with Brainphys media containing 1µM TTX. Following a 10

670 minute incubation in culture conditions, a further MEA recording was taken. Subsequently, the media

671 containing TTX was removed, and the organoid was washed 3 times with PBS, with fresh Brainphys

672 media added after the final wash. Following 2 hours in the incubator, a final recording was taken.

673 Results were produced by counting the spikes using a -5SD threshold after filtering, deriving an average

674 spike number for the whole MEA, deriving an average frequency for the whole MEA (by dividing the

675 spike number by recording time), and normalising each organoid's pre-, during and post-treatment

676 frequencies to the frequency of the organoid during the pre-treatment recording. Normalised values

677 were assessed for significance independently using a paired t-test, assuming similar distributions

678 between the two datasets.

679

680 ***Preparation of organoids and analysis by mass spectrometry***

681 Six organoids were isolated and cultured as previously described until week 10 after initiation of

682 differentiation. Three of these organoids were either cultured in CODM or BrainPhys medium for two

683 weeks. Medium was removed from organoids which were then homogenised and lysed with a drill and

684 pestle in 200 µl 2% SDS Lysis Buffer [2% (w/v) sodium dodecyl sulfate (SDS), 50 mM HEPES pH 7.4,

685 2 mM ethylene glycol-bis (β-aminoethyl ether)-N,N,N′,N′-tetraacetic acid (EGTA), 2 mM

686 ethylenediaminetetraacetic acid (EDTA), 2 mM phenylmethylsulfonyl fluoride (PMSF), EDTA-free

25

687   Protease Inhibitor (Roche) and PhosSTOP (Roche)] and freezing on dry ice. Frozen organoid lysate

688   was thawed and reduction was performed with 10 mM tris(2-carboxyethyl)phosphine (TCEP) at 85 °C

689   for 10 min with shaking. Samples were alkylated with 20 mM iodoacetamide for 30 min at 23 °C in the

690   dark. Protein was precipitated from using the chloroform-methanol method[11]. Protein pellet was

691   reconstituted in 20 µL of 7.8 M Urea, 50 mM HEPES pH 8.0. Protein was digested by the addition of 3

692   µg Lys-C (FUJIFILM Wako Pure Chemical Corporation) and incubation for 8 hours at 25 °C, 900 rpm.

693   Sample was then diluted 8-fold with 50 mM HEPES pH 8.0 and digested by the addition of 5 µg

694   TrypZean recombinant trypsin (Sigma-Aldrich) and incubation for 8 hours at 30 °C, with shaking. The

695   trypsin digestion was repeated for each sample. Protein content of each digest was estimated by

696   measuring the absorption of 280 nm light (Implen Nanophotometer, Labgear, Australia). 50 µg aliquots

697   of each sample were desalted on an in-house made STAGE tip with C18 material. Samples were eluted

698   in 50% acetonitrile, dried and then reconstituted in a solution of 90% acetonitrile, 0.1% trifluoroacetic

699   acid (TFA) for hydrophilic interaction chromatography (HILIC) fractionation.

700   HILIC fractionation was performed on a Dionex Ultimate 3000 HPLC system with a 250 mm long and 1

701   mm inside diameter TSKgel Amide-80 column (Tosoh Biosciences). HILIC gradient was between a

702   solution of 90% acetonitrile, 0.1% TFA (Buffer A) and a solution of 0.1% TFA (Buffer B). The sample

703   was injected into a 250 µl sample loop to be loaded onto the column at a flow rate of 60 µl/min in Buffer

704   A for 10 min. Gradient was from 100% Buffer A to 60% Buffer A (balanced with Buffer B) for 35 min at

705   a flow rate of 50 µl/min. Fractions were collected into a 96-well plate using a Probot (LC Packings) at 1-

706   minute intervals, monitored by absorbance of UV at 214 nm. UV signal was used to combine select

707   fractions into similar amounts of peptide. Fractions were dried and reconstituted in 0.1% formic acid for

708   LC-MS/MS analysis.

709   The LC-MS/MS was performed using a Dionex UltiMate 3000 RSLC nano system and Q Exactive Plus

710   hybrid quadrupole-orbitrap mass spectrometer (Thermo Fisher Scientific). The content of HILIC fractions

711   was loaded directly onto an in-house 300 × 0.075 mm column packed with ReproSil Pur C18 AQ 1.9

712   µm resin (Dr Maisch, Germany). The column was heated to 50 °C using a column oven (PRSO-V1,

713   Sonation lab solutions, Germany) integrated with the nano flex ion source with an electrospray operating

714   at 2.3 kV. The S lens radio frequency level was 60 and capillary temperature was 250 °C. The 5 µL

715   sample was injected into a 20 µl loop and loaded onto the column in 99% reversed phase buffer A

716   (solution of 0.1% formic acid) and 1% buffer B (solution of 0.1% formic acid, 90% acetonitrile) for 25 min

717   at 300 µL/min. The sample was loaded in 99% buffer A for 25 min. The gradient was from then from

718   99% buffer A to 95% buffer A in 1 min, to 75% buffer A in 75 min, to 35% buffer A in 8 min, to 1% buffer

719   A in 1 min, held at 1% buffer A for 2 min, to 99% buffer A in 1 min and held for 10 min. MS acquisition

720   was performed for the entire 120 min.

721 All samples and fractions were analysed using data-dependent acquisition LC-MS/MS. For data-

722 dependent acquisition, the MS scans were at a resolution of 70,000 with an automatic gain control target

723 of 1,000,000 for a maximum ion time of 100 ms from m/z 375 to 1500. The MS/MS scans were at a

724 resolution of 35,000 with an automatic gain control target of 200,000 and maximum ion time of 115 ms.

725 The loop count was 12, the isolation window was 1.2 m/z, the first mass was fixed at m/z 140 and the

726 normalized collision energy was 28. Singly charged ions and those with charge >8 were excluded from

727 MS/MS and dynamic exclusion was for 35 s.

728 The raw LC-MS/MS data was processed with MaxQuant v1.6.7.02[12] using the following settings:

729 variable modifications were oxidation (M), acetyl (protein N-terminus), deamidation (NQ);

730 carbamidomethyl (C) was a fixed modification; digestion was set to specific for trypsin with a maximum

731 of 3 missed cleavages; Label Free Quantification (LFQ) was enabled; Homo sapiens reference

732 proteome with canonical and isoform sequences downloaded March 9 2020 was used as well as the

733 inbuilt contaminants file; minimum peptide length was 7 and maximum peptide mass was 5000 Da;

734 second peptides search was enabled while dependent peptides searches were disabled; peptide

735 spectrum matching and protein false discovery rates were set at 1%; minimum score for modified

736 peptides was 40; all modified peptides and counterpart non-modified peptides were excluded from

737 protein quantification; matching between runs was disabled. All other parameters were default.

738 Entries in proteinGroups results file were filtered: CON_ and REV_ entries were removed; entries with

739 < 2 unique + razor peptides were removed; entries with no Intensity values were removed; entries for

740 which no gene name could be derived were removed. LFQ Intensity values for remaining entries was

741 used as input for an R script that used limma statistics to compare protein relative intensity

742 statistically.

743 The code for this script is reported here:

744 https://github.com/ChildrensMedicalResearchInstitute/MS_intensity_diffexpress.

745 The mass spectrometry proteomics data have been deposited to the ProteomeXchange Consortium

746 via the PRIDE[13] partner repository with the dataset identifier PXD025933 and 10.6019/PXD025933.

747

748 ***Gene ontology enrichment analysis of iPSC and cortical organoid proteomes***

749 The list of proteins detected by mass spectrometry were filtered to remove proteins that were not

750 detected in all three biological replicates. The number of "razor plus unique" peptides was required to

751 be two or greater using an average value across the three biological replicates. The filtered protein list

752 was converted to a gene list. Duplicate genes arising from multiple protein accession and isoforms were

753 filtered by removed the gene with the least number of "razor plus unique" peptides. Over-representation

754 analysis was conducted using WebGestalt. Significant enrichments for biological process and KEGG

755 pathway terms were determined by comparing to the human coding genome. The probability of

756 significant enrichment was adjusted using a false discovery rate of 5%.

757

758 ***AAV transduction of brain organoids***

759 AAV viral vectors (1-3.6x10E11 vg/organoid) were added to a total volume of 375 µl using fresh CODM

760 media used to culture the cortical and whole brain organoids. The organoids were then transferred to

761 low binding 24 well plates (Costar, Corning) and media was completely replaced with CODM containing

762 the AAV vectors. Cortical and whole brain organoids were incubated at 37 °C for half a day before

763 adding another 625 µl of fresh media. After overnight culture at 37 °C, the organoids and CODM/vector

764 mixture were transferred to a 60 mm dish. The dish was topped up to 4 ml with fresh CODM media and

765 put on an orbital shaker at 85 RPM at 37 °C. After 48 hours, organoids were fed every Monday,

766 Wednesday and Friday.

767

768 ***Statistical analysis***

769 All means are presented as mean ± SD (standard deviation) unless otherwise stated; N, number of

770 independent experiments i.e differentiation batches, proteome samples or MEA measurements; n,

771 number of images or retinal organoids examined, where appropriate. Statistical differences between two

772 groups were tested by two tailed paired and unpaired *t* tests. The preformed test is specified in figure

773 legends and main text. Statistical significance was assessed using Graphpad Prism software. Figures

774 were generated in Adobe Photoshop.

775

776 **Methods References**

777 1. Okita, K., Ichisaka, T. & Yamanaka, S. Generation of germline-competent induced pluripotent

778   stem cells. *Nature* **448,** 313–317 (2007).

779 2. Phillips, M. J. *et al.* Blood-derived human iPS cells generate optic vesicle-like structures with the

780   capacity to form retinal laminae and develop synapses. *Investigative Ophthalmology & Visual

781   Science* **53,** 2007–2019 (2012).

782 3. McGinnis, C. S. *et al.* MULTI-seq: sample multiplexing for single-cell RNA sequencing using

783   lipid-tagged indices. *Nat Methods* **16,** 619–626 (2019).

784 4. Tanaka, Y., Cakir, B., Xiang, Y., Sullivan, G. J. & Park, I.-H. Synthetic Analyses of Single-Cell

785   Transcriptomes from Multiple Brain Organoids and Fetal Brain. *Cell Rep* **30,** 1682–1689.e3

786   (2020).

787 5. Birey, F. *et al.* Assembly of functionally integrated human forebrain spheroids. *Nature* **545,** 54–

788   59 (2017).

789   6.   Velasco, S. *et al.* Individual brain organoids reproducibly form cell diversity of the human
790   cerebral cortex. *Nature* **570,** 523–527 (2019).

791   7.   Quadrato, G. *et al.* Cell diversity and network dynamics in photosensitive human brain
792   organoids. *Nature* **545,** 48–53 (2017).

793   8.   Trujillo, C. A. *et al.* Complex Oscillatory Waves Emerging from Cortical Organoids Model Early
794   Human Brain Network Development. *Stem Cell* 1–20 (2019). doi:10.1016/j.stem.2019.08.002

795   9.   Zhong, S. *et al.* A single-cell RNA-seq survey of the developmental landscape of the human
796   prefrontal cortex. *Nature* **555,** 524–528 (2018).

797   10.   Lin, Y. *et al.* scClassify: sample size estimation and multiscale classification of cells using single
798   and multiple reference. *Mol Syst Biol* **16,** e9389 (2020).

799   11.   Rappsilber, J., Ishihama, Y. & Mann, M. Stop and go extraction tips for matrix-assisted laser
800   desorption/ionization, nanoelectrospray, and LC/MS sample pretreatment in proteomics. *Anal*
801   *Chem* **75,** 663–670 (2003).

802   12.   Tyanova, S., Temu, T. & Cox, J. The MaxQuant computational platform for mass spectrometry-
803   based shotgun proteomics. *Nat Protoc* **11,** 2301–2319 (2016).

804   13.   Perez-Riverol Y, Csordas A, Bai J, et., al. The PRIDE database and related tools and
805   resources in 2019: improving support for quantification data. *Nucleic Acids Res* 47(D1):D442-
806   D450 (2019).

807
808   **Acknowledgments**

Author Contributions

Competing interests

References

1. Birey, F. *et al.* Assembly of functionally integrated human forebrain spheroids. *Nature* **545,** 54–59 (2017).
2. Qian, X. *et al.* Brain-Region-Specific Organoids Using Mini-bioreactors for Modeling ZIKV Exposure. *Cell* **165,** 1238–1254 (2016).
3. Gomes, A. R. *et al.* Modeling Rett Syndrome With Human Patient-Specific Forebrain Organoids. *Front Cell Dev Biol* **8,** 610427 (2020).
4. Ying, Q.-L., Stavridis, M., Griffiths, D., Li, M. & Smith, A. *Conversion of embryonic stem cells into neuroectodermal precursors in adherent monoculture. Nature Biotechnology* **21,** 183–186 (2003).
5. Chambers, S. M. *et al.* Highly efficient neural conversion of human ES and iPS cells by dual inhibition of SMAD signaling. *Nat Biotechnol* **27,** 275–280 (2009).
6. Paşca, A. M. *et al.* Functional cortical neurons and astrocytes from human pluripotent stem cells in 3D culture. *Nat Methods* **12,** 671–678 (2015).
7. Sinn, R. & Wittbrodt, J. An eye on eye development. *Mechanisms of Development* **130,** 347–358 (2013).
8. Lancaster, M. A. *et al.* Cerebral organoids model human brain development and microcephaly. *Nature* **501,** 373–379 (2013).
9. Lancaster, M. A. & Knoblich, J. A. Generation of cerebral organoids from human pluripotent stem cells. *Nat Protoc* **9,** 2329–2340 (2014).
10. Quadrato, G. *et al.* Cell diversity and network dynamics in photosensitive human brain organoids. *Nature* **545,** 48–53 (2017).
11. Qian, X., Song, H. & Ming, G.-L. Brain organoids: advances, applications and challenges. *Development* **146,** (2019).
12. Tanaka, Y., Cakir, B., Xiang, Y., Sullivan, G. J. & Park, I.-H. Synthetic Analyses of Single-Cell Transcriptomes from Multiple Brain Organoids and Fetal Brain. *Cell Rep* **30,** 1682–1689.e3 (2020).
13. Giandomenico, S. L. *et al.* Cerebral organoids at the air–liquid interface generate diverse nerve tracts with functional output. *Nat. Neurosci.* 1–17 (2019).
14. Zhong, S. *et al.* A single-cell RNA-seq survey of the developmental landscape of the human prefrontal cortex. *Nature* **555,** 524–528 (2018).

868 15. Trujillo, C. A. *et al.* Complex Oscillatory Waves Emerging from Cortical Organoids Model Early
869   Human Brain Network Development. *Stem Cell* 1–20 (2019).
870 16. Velasco, S. *et al.* Individual brain organoids reproducibly form cell diversity of the human
871   cerebral cortex. *Nature* **570,** 523–527 (2019).
872 17. Ning, A., Cui, J., To, E., Ashe, K. H. & Matsubara, J. Amyloid-beta deposits lead to retinal
873   degeneration in a mouse model of Alzheimer disease. *Investigative Ophthalmology & Visual*
874   *Science* **49,** 5136–5143 (2008).
875 18. Gupta, N., Ang, L.-C., Noël de Tilly, L., Bidaisee, L. & Yücel, Y. H. Human glaucoma and neural
876   degeneration in intracranial optic nerve, lateral geniculate nucleus, and visual cortex. *Br J*
877   *Ophthalmol* **90,** 674–678 (2006).
878 19. Reichman, S. *et al.* From confluent human iPS cells to self-forming neural retina and retinal
879   pigmented epithelium. *Proceedings of the National Academy of Sciences of the United States of*
880   *America* **111,** 8518–8523 (2014).
881 20. Reichman, S. *et al.* Generation of Storable Retinal Organoids and Retinal Pigmented Epithelium
882   from Adherent Human iPS Cells in Xeno-Free and Feeder-Free Conditions. *Stem Cells* **35,**
883   1176–1188 (2017).
884 21. Gonzalez Cordero, A. *et al.* Recapitulation of Human Retinal Development from Human
885   Pluripotent Stem Cells Generates Transplantable Populations of Cone Photoreceptors. *Stem*
886   *Cell Reports* **9,** 820–837 (2017).
887 22. Bardy, C. *et al.* Neuronal medium that supports basic synaptic functions and activity of human
888   neurons in vitro. *PNAS* **112,** E2725–34 (2015).
889 23. Lin, Y. *et al.* scClassify: sample size estimation and multiscale classification of cells using single
890   and multiple reference. *Mol Syst Biol* **16,** e9389 (2020).
891 24. Cesca, F., Baldelli, P., Valtorta, F. & Benfenati, F. The synapsins: Key actors of synapse
892   function and plasticity. *Progress in Neurobiology* **91,** 313–348 (2010).
893 25. Espuny-Camacho, I. *et al.* Pyramidal neurons derived from human pluripotent stem cells
894   integrate efficiently into mouse brain circuits in vivo. *Neuron* **77,** 440–456 (2013).
895 26. Bock, C. *et al.* Reference Maps of human ES and iPS cell variation enable high-throughput
896   characterization of pluripotent cell lines. *Cell* **144,** 439–452 (2011).
897 27. Nascimento, J. M. *et al.* Human Cerebral Organoids and Fetal Brain Tissue Share Proteomic
898   Similarities. *Front Cell Dev Biol* **7,** 303 (2019).
899 28. Zafeiriou, M.-P. *et al.* Developmental GABA polarity switch and neuronal plasticity in
900   Bioengineered Neuronal Organoids. *Nat Commun* **11,** 3791–12 (2020).
901 29. Zhao, X. & Bhattacharyya, A. Human Models Are Needed for Studying Human
902   Neurodevelopmental Disorders. *Am J Hum Genet* **103,** 829–857 (2018).
903 30. Kruczek, K. *et al.* Gene Therapy of Dominant CRX-Leber Congenital Amaurosis using Patient
904   Stem Cell-Derived Retinal Organoids. *Stem Cell Reports* **16,** 252–263 (2021).
905 31. Kallman, A. *et al.* Investigating cone photoreceptor development using patient-derived NRL null
906   retinal organoids. *Commun Biol* **3,** 82–13 (2020).
907 32. Lane, A. *et al.* Modeling and Rescue of RP2 Retinitis Pigmentosa Using iPSC-Derived Retinal
908   Organoids. *Stem Cell Reports* **15,** 67–79 (2020).
909 33. Lukovic, D. *et al.* Retinal Organoids derived from hiPSCs of an AIPL1-LCA Patient Maintain
910   Cytoarchitecture despite Reduced levels of Mutant AIPL1. *Sci Rep* **10,** 5426–13 (2020).
911 34. Guo, Y. *et al.* Modeling Retinitis Pigmentosa: Retinal Organoids Generated From the iPSCs of a
912   Patient With the USH2A Mutation Show Early Developmental Abnormalities. *Front Cell*
913   *Neurosci* **13,** 361 (2019).
914 35. Quinn, P. M. *et al.* Human iPSC-Derived Retinas Recapitulate the Fetal CRB1 CRB2 Complex
915   Formation and Demonstrate that Photoreceptors and Müller Glia Are Targets of AAV5. *Stem*
916   *Cell Reports* **12,** 906–919 (2019).
917 36. Deng, W.-L. *et al.* Gene Correction Reverses Ciliopathy and Photoreceptor Loss in iPSC-
918   Derived Retinal Organoids from Retinitis Pigmentosa Patients. *Stem Cell Reports* **10,** 1267–
919   1281 (2018).

37. Megaw, R. *et al.* Gelsolin dysfunction causes photoreceptor loss in induced pluripotent cell and animal retinitis pigmentosa models. *Nat Commun* **8,** 271 (2017).

38. Parfitt, D. A. *et al.* Identification and Correction of Mechanisms Underlying Inherited Blindness in Human iPSC-Derived Optic Cups. *Cell stem cell* **18,** 769–781 (2016).

39. Andersen, J. *et al.* Generation of Functional Human 3D Cortico-Motor Assembloids. *Cell* **183,** 1913–1929.e26 (2020).

40. Xiang, Y. *et al.* hESC-Derived Thalamic Organoids Form Reciprocal Projections When Fused with Cortical Organoids. *Stem Cell* **24,** 487–497.e7 (2019).

41. Bagley, J. A., Reumann, D., Bian, S., Lévi-Strauss, J. & Knoblich, J. A. Fused cerebral organoids model interactions between brain regions. *Nat Methods* **14,** 743–751 (2017).

42. Miura, Y. *et al.* Generation of human striatal organoids and cortico-striatal assembloids from human pluripotent stem cells. *Nat Biotechnol* **38,** 1421–1430 (2020).

43. Hadoux, X. *et al.* Non-invasive in vivo hyperspectral imaging of the retina for potential biomarker use in Alzheimer's disease. *Nat Commun* **10,** 4227–12 (2019).

Supplementary information
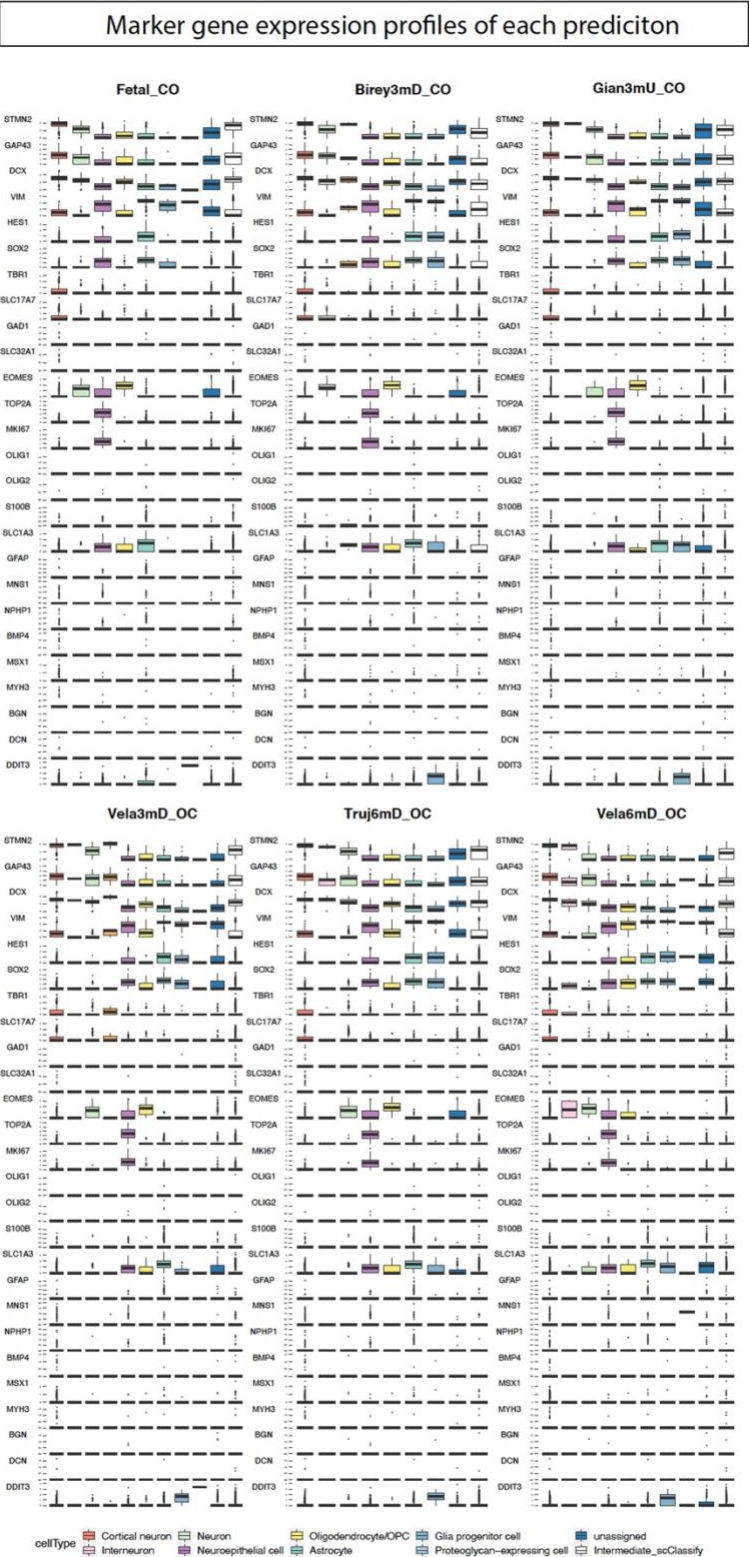
Supplementary Figures
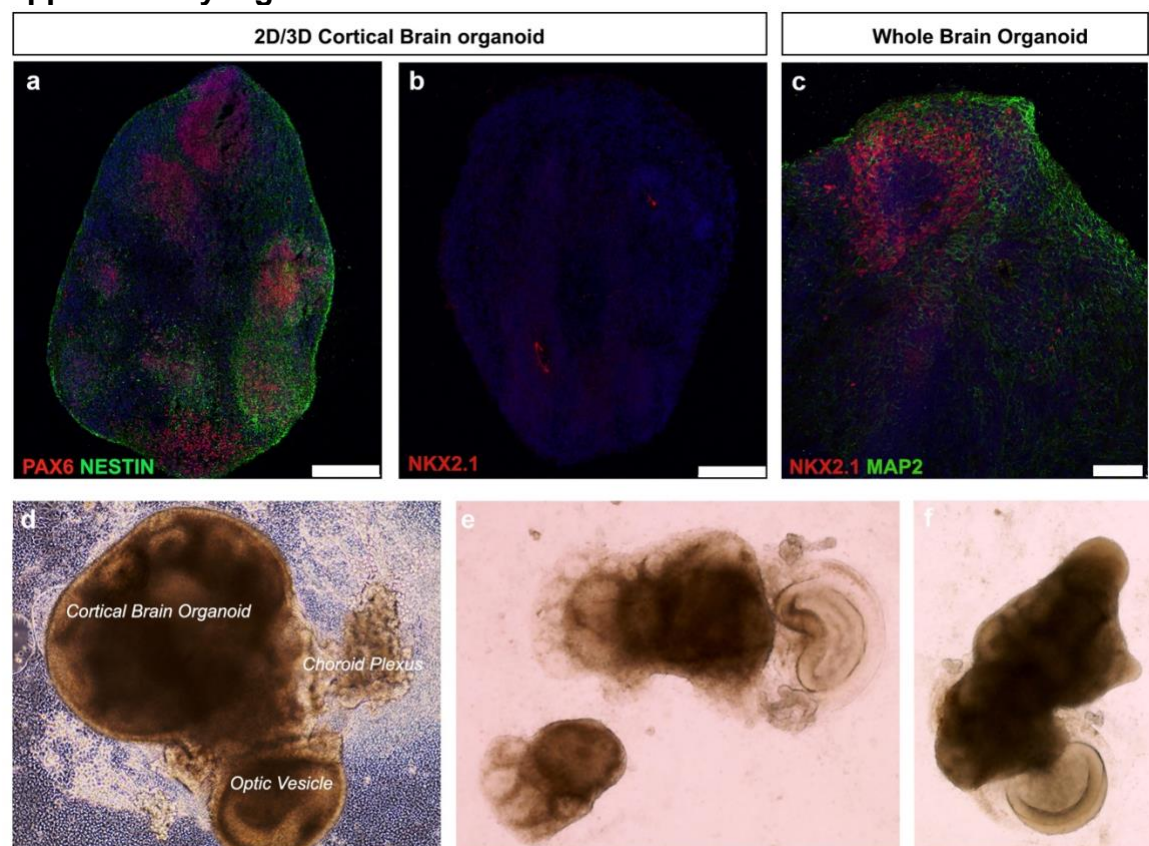
Supplementary Figure 1. Confluent iPS differentiation protocol gives rise to cortical and retinal organoids. **a.** Immunohistochemistry image showing PAX6 and NESTIN positive cortical organoid. **b.** Image showing that cortical organoid negative for ventral cortex marker, NKX2.1. **c.** Image showing NKX2.1 and MAP2 positive whole brain organoid. **d-f.** Bright field imaged showing examples of cortical brain organoids growing in proximity to optic vesicles. Scale bars, 75 μm (c), 250 μm (a, b).

947

948

949

950

951

952

953

954

955

956

957

958

959
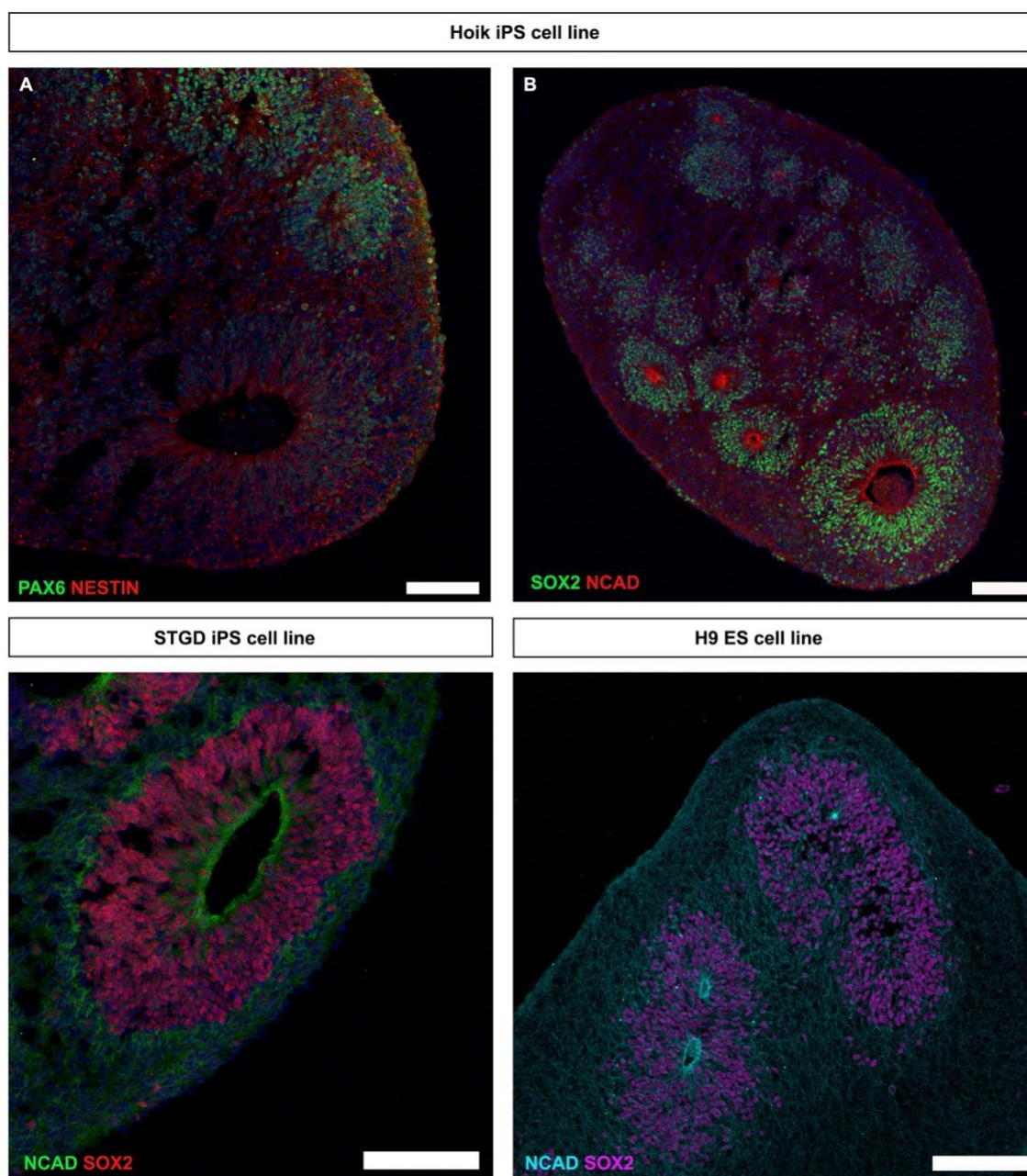
Supplementary Figure 2. Early cortical organoids derived from various iPSC lines. a-d. Representative images of early neural markers of cortical organoids generated from iPSC lines and ES cell line H9. Scale bars, 100μm (a-d).

Supplementary Figure 3. Marker gene expression profile for each scRNA-seq available datasets.
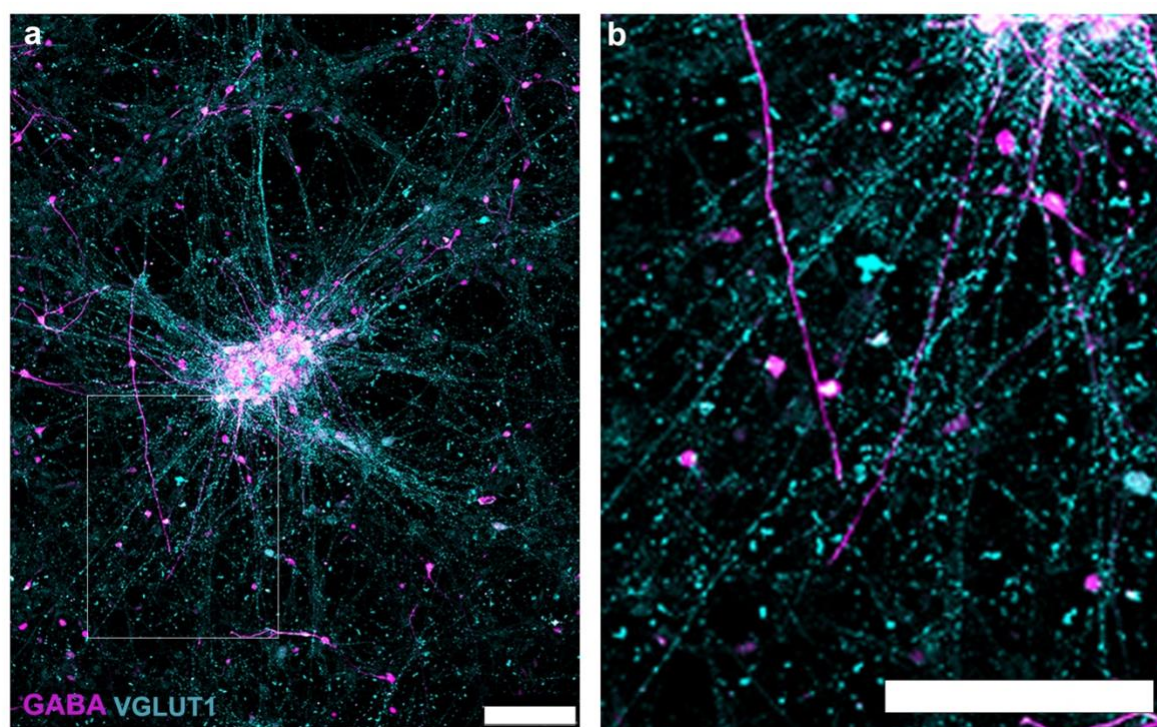
967
968
969 **Supplementary Figure 4. 2D cultures of cortical neurons dissociated from brain**
970 **organoids. a, b.** Immunohistochemistry image showing GABA inhibitory neurons and
971 VGLUT1 inhibitory neurons. b is the high magnification image of inset in a. Scale bars, 100
972 μm (a, b).
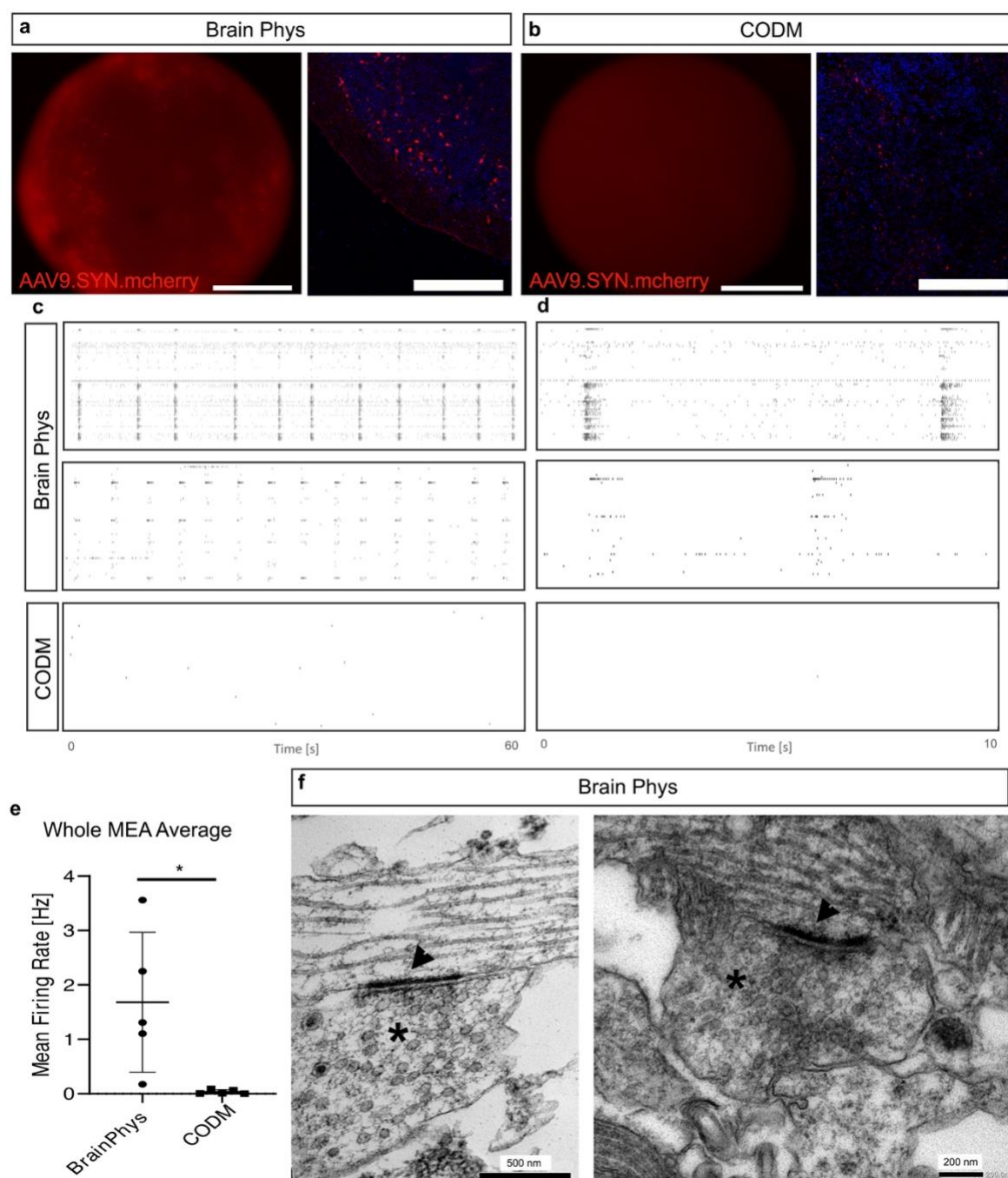
973
Supplementary Figure 5.
a, b. Representative bright field and immunohistochemistry images showing brain Phys and CODM cultured cortical organoids transduced with AAV9.SYN.mcherry viral vectors. **c, d.** Representative spike raster plots showing firing patterns of organoids across all electrodes with marked network bursts in Brain Phys, but not in CODM cultured organoids. **e.** whole MEA mean firing rate activity (mean ± SD, paired *t* test, * p<0.01). **f.** Ultrastructure electron microscopy images of Brain Phys cultured cortical organoid showing synaptic clefts (head arrows) and synaptic vesicles (asterisks). Scale bars, 250 μm (a, b)
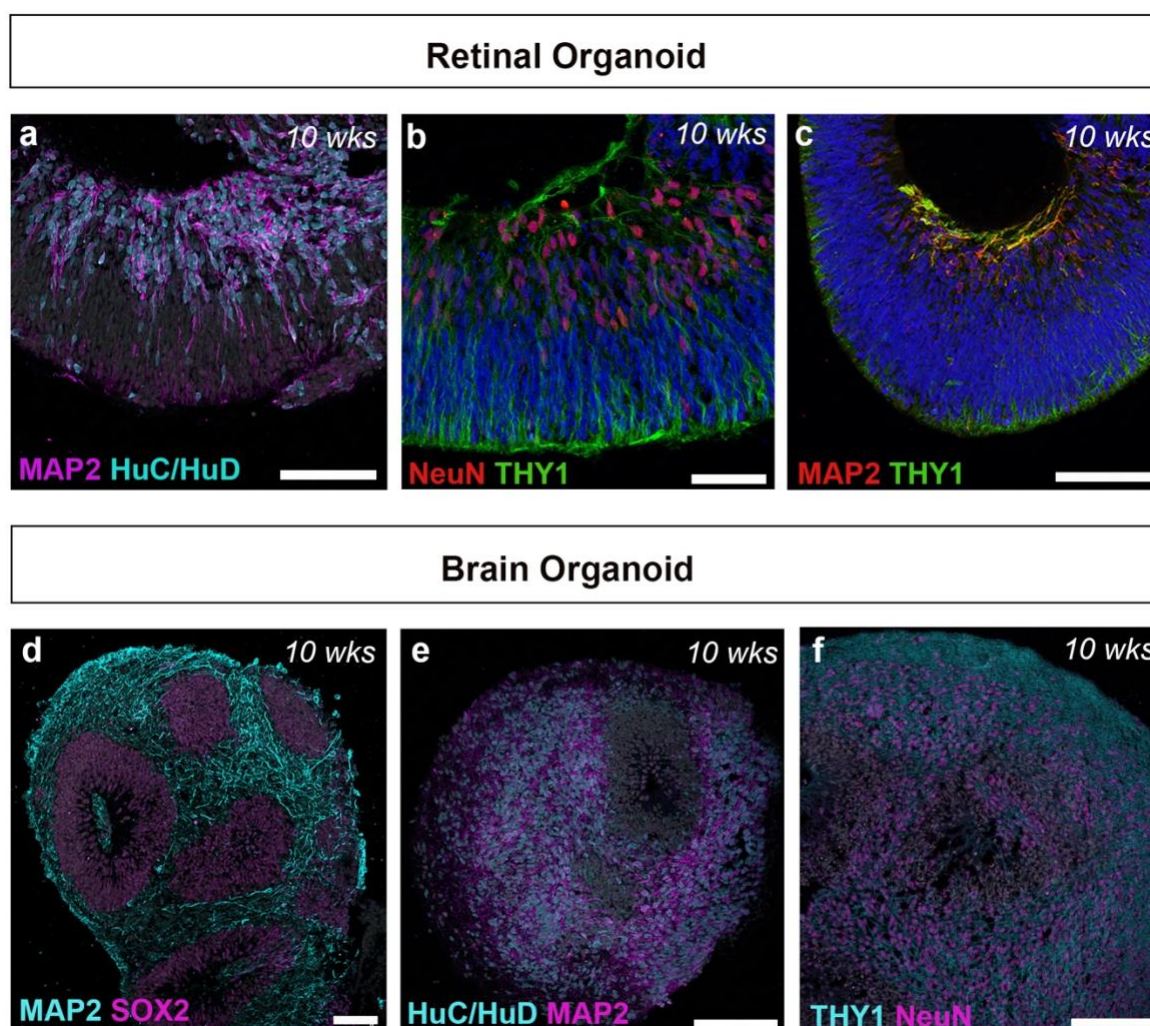
Supplementary Figure 6. Neuronal markers on both retinal and brain organoids. a-f. Representative immunohistochemistry images from 10 weeks old retinal and cortical brain retinal organoids. a-c. Typical interneurons and retinal ganglion cell cells markers in the basal layer of the retinal organoid. **d-f.** The same markers are also expressed in cortical neurons of brain organoids. Scale bars, 75 μm (d), 150 μm (a, b, c, e, f).

Supplementary Movies Legends

SMovie 1. Differentiation of early cortical progenitors
Video of a typical representative day 35 cortical organoid showing neuroepithelium regions positive for PAX6 (red) and NESTIN (green). DAPI stained in blue.

SMovie 2. Differentiation of neurons and glial cells
Lightsheet video of a cleared whole cortical organoid at day 75 in culture. Organoid showing numerous neurons positive for CALRETININ (red) and glial cells positive for SB100 (green). DAPI stained in blue.

SMovie 3. Optic nerve-like formation between retinal and cortical organoids

1001 Lightsheet video of cleared retinal-brain complex organoids. Video showing 510 z stacks
1002 starting at the retinal organoid with typical thick neuroepithelia showing MAP2 positive retinal
1003 ganglion cells and axonal projections leading towards cortical organoid with neurons positive
1004 for MAP2.

1005

Supplementary Table 1. Antibodies used for immunohistochemistry			
Antigen	Host species	Concentration used	Supplier
Calretinin	mouse	1 in 200	Merck Millipore (MAB1568)
Caspase3	rabbit	1 in 200	Abcam (ab2302)
Ctip2	rat	1 in 200	Abcam (Ab18465)
FoxG1	rabbit	1 in 200	Abcam (Ab18259)
GABA	rabbit	1 in 200	Sigma (A2052)
GFAP	rat	1 in 200	Sigma (345860)
Ki67	rabbit	1 in 200	Abcam (ab15580)
MAP2	chicken	1 in 1000	Abcam (ab5392)
MAP2	mouse	1 in 200	Merck Millipore (MAB3418)
NCAD	mouse	1 in 200	BD Bioscience (610921)
Nestin	mouse	1 in 200	Merck Millipore (MAB5326)
Pax6	rabbit	1 in 200	Bioscience (901302)
PSD95	goat	1 in 200	Abcam (ab12093)
Satb2	rabbit	1 in 200	Abcam (Ab34735)
SB100	mouse	1 in 200	Sigma (S2532)
Sox2	rabbit	1 in 200	Abcam (ab97959)
Sox2	mouse	1 in 200	BD (561469)
Synaptophysin	mouse	1 in 200	Abcam (ab8049)
TBR1	rabbit	1 in 200	Abcam (ab31940)
Tuj1	mouse	1 in 2000	Thermo Fisher Scientific (MA1118X)
Vglut1	Guinea pig	1 in 200	Merck Millipore (AB5905)

1006